SHAPE-BASED INSECT CLASSIFICATION: A

HYBRID REGION-BASED AND CONTOUR-BASED

APPROACH

By

BO LI

Bachelor of Science in Electronic Information Science

and Technology

Shandong University

Jinan, Shandong, China

2009

Submitted to the Faculty of the
Graduate College of the
Oklahoma State University
in partial fulfillment of
the requirements for
the Degree of
MASTER OF SCIENCE
July, 2014

SHAPE-BASED INSECT CLASSIFICATION: A

HYBRID REGION-BASED AND CONTOUR-BASED

APPROACH

Thesis Approved:

Dr. Guoliang Fan

Thesis Adviser

Dr. James Hardin

Thesis Co-Adviser

Dr. Damon M. Chandler

ACKNOWLEDGEMENTS

At the moment of finishing this work, I would like to express my sincere thanks to those who have provided me help in the course of writing this thesis. First of all, I would express sincere appreciation to my advisor, Dr. Guoliang Fan. Definitely without his great help and kind encouragement I would not have the opportunity to successfully finish this research. Secondly, I would like to thank my co-advisor, Dr. James Hardin, who has given me tremendous help on work direction and so much advice on thesis writing. I would also like to thank my committee member Dr. Damon Chandler. Through lively discussions I gained valuable knowledge in my research. I would like to give special thanks to Dr. Hairong Liu, the author of the paper on Visual Curvature [1] who gave me great support for the implementation of the visual curvature algorithm. In addition, I would like to thank XTO Energy Incorporated which generously provided financial support for this research.

Finally, I would like to thank my dear parents. I deeply understand that you are standing behind me forever. Your support encouraged me through the most difficult time.

Name: Bo Li

Date of Degree: July, 2014

Title of Study: SHAPE-BASED INSECT CLASSIFICATION: A HYBRID REGION-
BASED AND CONTOUR-BASED APPROACH

Major Field: Electrical Engineering

Abstract: The American Burying Beetle (ABB) (*Nicrophorus americanus*) is a critically endangered insect whose distribution is limited to several states at the periphery of its historical range in the eastern and central United States. The objective of this study is to develop a digital image classification algorithm that will be used in an autonomous monitoring system to be attached to existing ABB traps that will detect, image, classify and report insects to species as they enter the trap. A training set of 92 individual specimens representing 11 insect species with shape similarity from the Oklahoma State University Entomology Museum was used in this study. Starting with a color digital image, an unsupervised preprocessing algorithm extracts each insect shape, converts it to a binary image, and then aligns it for classification using pattern recognition techniques. For region-based and contour-based shape representation methods, an area component and a Fourier descriptor methods are implemented for shape representation and classification. Analysis of initial classification results revealed that the pose variability of insect legs and antennae introduced excessive uncertainty in the feature space. To address this, a novel shape decomposition algorithm based on curvature theory is proposed to remove legs and antennae from the insect shape automatically prior to classification. This shape decomposition approach increased overall classification accuracy from 64% to 76% and 57% to 67% for area component and Fourier descriptor methods respectively. To further improve classification accuracy, a hybrid approach using a decision fusion technique has also been implemented after initial classification by each method. This resulted in 100% classification accuracy for ABB and 90% overall classification accuracy for the 11 species (total 92 images) investigated.

TABLE OF CONTENTS

LIST OF TABLES

LIST OF FIGURES

CHAPTER I

INTRODUCTION

1.1 Background and Motivation

The American Burying Beetle (ABB) (*Nicrophorus americanus*) (Figure 1.1) is classified as a

critically endangered species by the U.S. Fish and Wildlife Service (USFWS). The historic range

of ABB was the Eastern US but it is currently only found in three small areas of the United States

centered in eastern Oklahoma, central Nebraska and Block Island in Rhode Island [2]. Ongoing

research projects at Oklahoma State University, Murray State University and other organizations

are investigating ABB biology and ecology with the aim to identify methods to insure survival of

the species. These research studies, and existing USFWS monitoring and management protocols,

entail extensive trapping of ABB and related insect species. Current ABB trapping methods

require daily, early morning monitoring of traps to check whether any beetles were captured

overnight. This is labor intensive and limited temporal data is provided because most beetle

activity occurs at night.

Figure 1.1: American Burying Beetle (ABB) [3].

A research project is underway to develop an autonomous monitoring system that can be attached to existing ABB traps. The trap monitor incorporates a cellular phone which runs an Android™ application that contains primary trap functions. The application detects when an insect enters the trap, takes a dorsal image of the insect and classifies it as ABB or other species. If the insect is classified as an ABB, a simple/multimedia message service alert containing GPS coordinates, time stamp, an image and other data will be sent out over the cell phone network to alert collection personnel. This improved trap has potential to dramatically reduce labor costs, improve data richness, and reduce stress on captured ABB by immediately alerting personnel of trapped insects [4].

1.2 Objective and Approach

The specific objective of this research project is to develop robust image segmentation and classification algorithms for the autonomous ABB trap. The classification capability must include ABB and other species of interest routinely caught in the traps. Due to the protected status of ABB, the algorithm was developed and tested the using dead specimens from Oklahoma State University's Entomology Museum. The training database consisted of insect specimens

comprising 11 species with a total of 92 individuals, most of which have shape similarity

discerned by human vision (Table 1.1). There were 10 ABB specimens in the training database.

Species	ID	Number of individuals	Representative image
Nicrophorus americanus (ABB)	S1	10	
Necrodes americana	S2	9	
Necrodes surinamensis	S3	10	
Nicrophorus carolinus	S4	10	
Nicrophorus pustulatus	S5	6	
Nicrophorus tomentosus	S6	6	
Nicrophorus marginatus	S7	10	
Nicrophorus orbicollis	S8	6	
Oiceoptoma inaequale	S9	9	
Creophilus maxillosus	S10	8	
Creophilus maculosus	S11	8	

Table 1.1: Species used in classification.

The input images for this study were color digital images of the insect specimens positioned dorsal side up on a mounting board. Variations among them on size, pose, color and shape are significant factors to be investigated by the algorithm. Specifically, this investigation focused on shape analysis of binary images. In order to extract features precisely from a binary image, it is imperative that the images be composed using similar criteria. Thus our initial effort was to apply appropriate morphological operations and develop an extraction and alignment algorithm for individual insect images. After each insect image is composed in a similar manner, its shape is represented by feature vectors using region-based and contour-based methods. Corresponding to these two methods, area components and Fourier Descriptors are applied to classify insects to species using a template matching technique. Initial classification accuracies using composed images were relatively low: 45% for ABB and 61% overall. Analysis of the initial classification results led to the hypothesis that significant shape uncertainty was introduced by variation in the pose of legs and antennae among the different specimens. For example, the legs and antennae were attached to the insect body shape in some individuals while fully expanded in others. This hypothesis was confirmed when the same shape representation methods increased classification accuracy by 70% for ABB and 75% overall respectively after legs and antennae were manually removed from binary insect shape images. An unsupervised method to identify and ultimately remove legs and antennae was therefore desired.

Several shape decomposition methods have been previously proposed based on convexity and concavity rules [5-8], however the insect shape is distinctive because of its non-smooth shape contour curve and irregular details. To address this challenge, a new shape decomposition method was proposed to remove insect shape uncertainty based on visual curvature [1]. This method first identifies a candidate cut set from points that have a large visual curvature. After making observations on reasonable cuts according to human vision, several intrinsic properties were determined which reduced the size of the candidate cut set. Next the largest closed curve area is

removed which is comprised of the cut itself and a partial shape contour. The candidate cut set is dynamically renewed after each cut and the algorithm is repeated until enough reasonable cuts are accomplished. Based on the auto-decomposed shape, overall classification accuracies using area components and Fourier descriptors were both significantly improved to 76% for ABB and 67% overall.

Analysis of misclassified cases from each approach revealed that the two methods were complementary to each other suggesting that a decision fusion technique might improve classification accuracy. The minimum Euclidean distance between the feature vector of an unknown insect shape and the mean feature vector of the various species is used to classify each individual to species. It is straight forward to apply fuzzy set theory to classify unknown shapes after normalization of the Euclidean distances to all of the other mean shapes. Hence, a decision combination rule proposed by Fauvel et al. [9] was implemented to methodically combine the decisions of the two classification methods. By doing this, overall classification accuracy of 90%, and ABB classification accuracy of 100% was ultimately achieved for this sample set.

1.3 Main Contribution

An autonomous insect classification system presents many fundamental computer vision challenges exaggerated by the articulated body parts (legs, antennae, wings, abdomen, etc.) of insects [10]. Legs and antennae in particular introduce uncertainty when using insect shape features for classification. To the best of our knowledge, there is no existing specific method in use or proposed for the treatment of insect legs and antennae in an autonomous insect classification system.

Based on observations of shape distortion introduced by insect legs and antennae, we proposed a novel shape decomposition algorithm to preserve the main body shape for species classification. The algorithm automatically identifies cuts to remove legs and antennae from the insect shape

5

thus enhancing the function of the autonomous insect classification algorithm. This algorithm is not specific to ABB and is widely adaptable to all species in our training database. In addition, the decomposed shape could be universally used when applying other shape representation methods, or even color-related representation methods, in the future.

This thesis is organized as follows: Chapter 2 discusses existing insect classification and recognition work using pattern recognition, relevant classical shape representation methods using both region-based and contour-based approaches as well as existing shape decomposition procedures based on convexity and concavity rules. Chapter 3 describes the image preprocessing procedures including insect object segmentation and alignment as well as a region-based shape representation method for classification. The effect on classification results using a dimension reduction technology, principal component analysis (PCA), is also discussed. In Chapter 4, Fourier descriptor theory [11] is presented as a contour-based shape representation method. Visual curvature, proposed by Liu et al. [1] is also discussed as the foundation of the shape decomposition algorithm. Most importantly, our novel intuitive insect shape decomposition method is presented in detail followed by experimental results and analysis. Chapter 5 presents the hybrid region-based and contour-based approach based on fuzzy set theory using decision fusion technology. Chapter 6 evaluates the overall performance of this autonomous insect classification system and summarizes the conclusions.

CHAPTER II

RELATED WORK

A brief overview of previous related work follows. In particular, a review of the literature is

presented on image-based automatic insect species classification. Following that, region-based

and contour-based shape representation approaches based on analysis of shape features are

reviewed and discussed. Finally, as an important step toward shape understanding, shape

segmentation and decomposition methods are discussed [5].

2.1 Machine Vision for Insect Classification

Autonomous computer vision and pattern recognition methods have been widely investigated to

improve efficiency and accuracy of many environmental applications involving imagery. This

includes classification and identification of many insect species in a variety of different

applications.

After preprocessing procedures are applied to the original captured image, there are numerous

feature selection algorithms for classification to choose from. When using color images, the most

common approach is to analyze the color components. Cho et al. [12] used the average color

intensity values for red, green, and blue color components as the feature to classify Whiteflies,

Aphids and Thrips found in greenhouses. Mayo et al. [13] extracted color features not only in

RGB color space, but also in HSB color space for classification of live moths. At the same time,

instead of analyzing the entire body, their method concentrated on the centroid grid of moths for

binary feature extraction. Another interesting method proposed by Zayas et al. [14] was to find

specific beetle species in wheat samples using a patch color feature matching method in RGB and HSL color spaces. In general, color components analysis methods are not robust when images are captured in different surroundings or conditions. In addition, with many insect species exhibiting color similarity, the method is not able to classify them to a high degree of accuracy.

Based on binary images, shape information provides an important feature for object classification and recognition. Numerous shape feature extraction methods have been thoroughly studied for both region-based and contour-based shape representation approaches. Al-Saqer et al. [15] applied five recognition methods for Pecan Weevil identification based on template matching technology, including normalized cross-correlation, Fourier descriptors, Zernike moments, string matching and regional properties. When the recognition methods were applied in a specific order, this method could achieve relatively high identification accuracy. However this specific order for classification methods and numerous parameter selections make application to other systems difficult. Arbuckle et al. [16] proposed a recognition system for bees based on the patterns found on their wings. This method required human interaction to do preprocessing work on the wings before image analysis. Watson et al. [17] proposed a system for insect classification of several moth species. However, it was not an autonomous system due to the requirement of human intervention to align the insects. In addition, this system required a large training database which made its application inefficient. Larios et al. [10] described an automatic computer vision classification approach, but it was applicable only to stonefly larvae. After the identification of regions of interest, this method used the histogram features of SIFT vectors [18] on those regions for classification.

2.2 Shape Representation Methods

Shape representation methods can generally be classified into two categories: region-based and contour-based approaches. Shape features are extracted from the entire shape region in region-

based methods whereas shape features are extracted only from the outline of the shape in contour-based methods. A good shape representation method should be effective in finding perceptually similar shapes in various complex circumstances, such as shape rotation, translation and scaling, curve defining point shifts, noise affected shapes, distorted shapes and defective shapes [19].

2.2.1 Region-based Shape Representation Methods

Hu [20] first proposed a theory of two-dimensional moment invariants of planar geometric figures in 1961, and this concept was applied to shape classification and retrieval by Ezer et al. [21] and Park et al. [22]. This set of seven 2-D moment invariants are insensitive to shape rotation, translation and change of scale [23]. Zernike moments, proposed by Khotanzad et al. [24], are a mapping of an image shape onto a set of orthogonal basis functions over the unit circle. The magnitudes of a set of orthogonal complex moments represent the shape feature with rotational invariance. Based on Zernike moments, Li et al. [25] proposed the invariant Zernike moments descriptor, which not only uses magnitude information of the orthogonal complex moments, but also combines phase coefficients to form the shape descriptor. This descriptor is unaffected by shape rotation, translation and scaling. Bunke et al. [26] presented a string matching method for 2-D shape recognition. This method is pixel oriented and is based on curvature. It requires fewer computer resources for preprocessing but more in the matching algorithm. Kim et al. [27], introduced the idea of using a combination of sub-region features. The whole shape is divided into several segments by two principle axes then several parameters are calculated to represent each region. The entire shape feature is an arrangement of the calculated features in all sub-regions. Another interesting method is proposed by Zhang et al. [28] who used a contour-based method to compute a concentric circular sampling signature in a shape region which could achieve rotation, translation and scaling invariance as well.

2.2.2 Contour-based Shape Representation Methods

The Fourier descriptor [11] is one of the most widely used algorithms for shape representation and classification in the contour-based shape representation category. The Fourier descriptor is determined by applying the discrete Fourier transform (DFT) to the complex sequence associated with the boundary curve. Numerous variations based on the Fourier descriptor of shape contours have been proposed. These include an affine Fourier descriptor with affine transformation invariance proposed by Arbter [29] using a complex mathematical analysis, the modified Fourier descriptor with insignificant properties separation proposed by Granlund [30] for hand print character recognition, fastest point distance including corner information proposed by El-ghazal et al. [31] and angular radius Fourier descriptor combining the directional angle of the boundary line proposed by Kunttu et al. [32]. Besides Fourier descriptors, Yang et al. [33] proposed the starting-point-independent wavelet descriptor for 2-D shape recognition consisting of the estimation of the misalignment between the starting points for the reference model and matching objects using multiresolutional wavelet representation. Belongie et al. [34, 35] proposed the shape context descriptor, which for each point captures the distribution of the remaining points relative to it. Shape context solves for correspondence between points on the two shapes. Corresponding points on two similar shapes will have similar shape contexts, which make it robust for measuring shape similarity once shapes are aligned. Freeman [36] proposed the chain code concept to describe an object in 1961. The shape descriptor is a sequence of small vectors of unit length containing pre-defined possible direction information. Lee et al. [37] proposed a polygon curve evolution algorithm for smoothing polygon curves and reducing the number of data points while keeping the main topology of the shape. The curve is represented by a bend angle versus normalized curvature length function derived from the x and y coordinates of the boundary points. Arica et al. [38] proposed an image retrieval algorithm which finds similar objects in a database based on a discrete circular Hidden Markov Model. This model is size and starting point shift invariant as well as requiring less computational complexity compared to other methodologies.

10

2.3 Shape Decomposition

Shape decomposition is a fundamental problem in handling shapes in a variety of disciplines, such as computer vision, data visualization and computer graphics [5]. In shape decomposition methods, the convexity rule is the most widely used criteria in object segmentation. By identifying the convex parts at different stages, Latecki et al. [6] proposed a contour evolution method to make significant visual parts at higher stages when they become convex object parts. A hierarchical convexity rule is then used for shape decomposition where visual parts are enclosed by the maximal convex object at different stages of the contour evolution. With the definition of cut cost, Liu et al. [5] formalized the convex shape decomposition problem as an integer linear programming problem, and the approximate optimal decomposition solution is obtained by minimizing the total cost under some concavity constraints. Based on that work, Ren et al. [7] proposed the near-convex decomposition algorithm where the degree of near-convexity specified by the user is used to decompose 2-D and 3-D arbitrary shapes into a minimum number of parts. Using the non-overlapping cut constraints and by imposing perception rules, the shape decomposition problem is formulated as a combinational optimization problem. Ghosh et al. [8] proposed Fast Approximate Convex Decomposition which employed two new strategies. The first strategy is that each potential cut is evaluated by the relative reduction in concavity it produces rather than absolute concavity. The second strategy uses a dynamic programming approach to select a set of candidate cuts satisfying a non-crossing constraint. The two strategies are used simultaneously to decompose the shape. Kim et al. [39] proposed an algorithm which performs constrained morphological decomposition recursively. The opening morphological operation is used for shape processing and the optimal decomposition is selected by weighted convexity. In other work, Mi et al. [40] proposed a model for separating 2-D parts based on differential geometry of smoothed local symmetries and relatability. The criterion used for cut

selection is to make either the remaining shape or the segment removed to be a simpler shape. The relatability is taken into account to determine part boundaries.

2.4 Our Approach and Advantages

In this investigation, we propose an insect classification system which includes these advantages: automatic application, few algorithm parameter selections and robust properties for classification of numerous species. Specifically, using pre-set parameters, an insect image is classified to species by progressing through a sequence of image preprocessing, feature extraction, shape decomposition, classification by multiple classifiers and a final decision fusion step. In the image preprocessing step, human intersection is not required. To describe the shape precisely, both region-based and contour-based shape representation methods are used for feature extraction. Specifically, an area component method is applied in the region-based category whereas Fourier descriptors are utilized in the contour-based category. Based on marginal initial classification results obtained from our training set, a novel shape decomposition algorithm is proposed to automatically remove shape uncertainty introduced by legs and antennae, which results in increased classification accuracies. After classification by each method independently, a hybrid region-based and contour-based approach using decision fusion technology is implemented in this system to improve performance.

CHAPTER III

REGION-BASED SHAPE REPRESENTATION

The initial color images of captured insects are in general not suitable for classification directly. Several external factors influence the ability to analyze color images such as lighting, weather conditions and the camera itself. In binary images, where we generally focus on shape analysis without regard to color components, background noise and object pose can still have significant effects on the shape representation. To maintain shape information accuracy in preparation for classification, several image preprocessing procedures such as morphological operations, object segmentation and object alignment are first required. After image preprocessing, the binary shape images are classified using a region-based approach. This chapter describes the image preprocessing steps and presents the subsequent insect classification results obtained using region properties.

3.1 Image Preprocessing

The ultimate objective of this research is the unsupervised classification to species of images of insects taken by a cell phone camera located in a trap. The input images for this project were digital camera images of dead insects positioned dorsal side up on a mounting board (Figure 3.1). Each JPEG input image contained several insect specimens on a non-noiseless, white background. In addition, the insects were posed at various angles and directions which dictates that the algorithm be able to deal with each insect specimen individually to place them in the same presentation criteria. The output of the image preprocessing step was an individual binary

insect image aligned along its longitudinal axis.

Figure 3.1: Representative unprocessed color JPEG image of insect (ABB) specimens.

3.1.1 Object Segmentation

Binary images have several advantages over color and gray scale images for insect shape analysis through image processing. Binary images generally require less storage space, allow for faster processing speed and have straightforward algorithm implementations which are desirable in this application. The first step in segmentation is to convert the input image from a color JPEG format to a binary image. The insect specimens mounted on a white surface in this study had sufficient contrast between the object and the background to allow the binary image to preserve the insect body shape precisely using a threshold which was automatically calculated by the program (Figure 3.2). Each insect body shape closely resembles the outline of the corresponding color image with some uncertainty due to noise caused by reflections, shadows and pixelization.
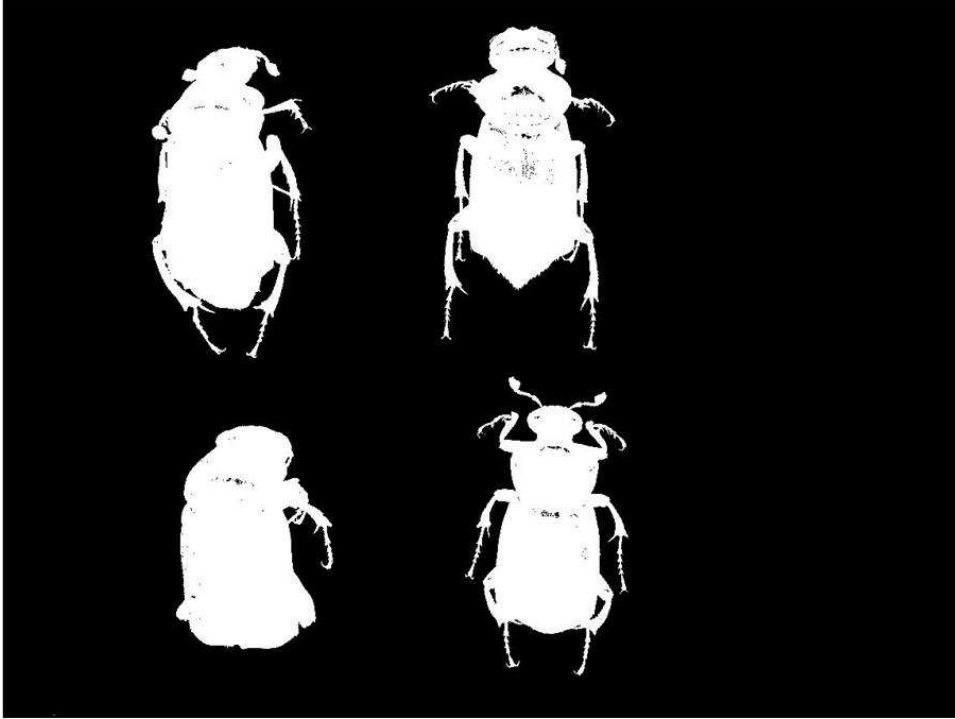
Figure 3.2: Representative binary image of insect specimens calculated from threshold operation.

Several morphological operations are required to prepare the binary images that result from the threshold operation for classification. The first operation is to fill holes in the binary images using the hole filling operation. For the object and background in the binary image, the operation sets the binary image f_m, to be a 0 everywhere except inside the image border, where it is set to $1 - f$ [23].

$$f_m(x, y) = \begin{cases} 1 - f(x, y), & \text{if } (x, y) \text{ is in the border of } f \\ 0, & \text{otherwise} \end{cases}$$ (3.1)

The second operation is to step through each pixel in the binary image and label each pixel p as a foreground pixel if at least five pixels of its 8 nearest neighbors (Figure 3.4(b)) are foreground pixels; otherwise it is labeled as a background pixel [23].
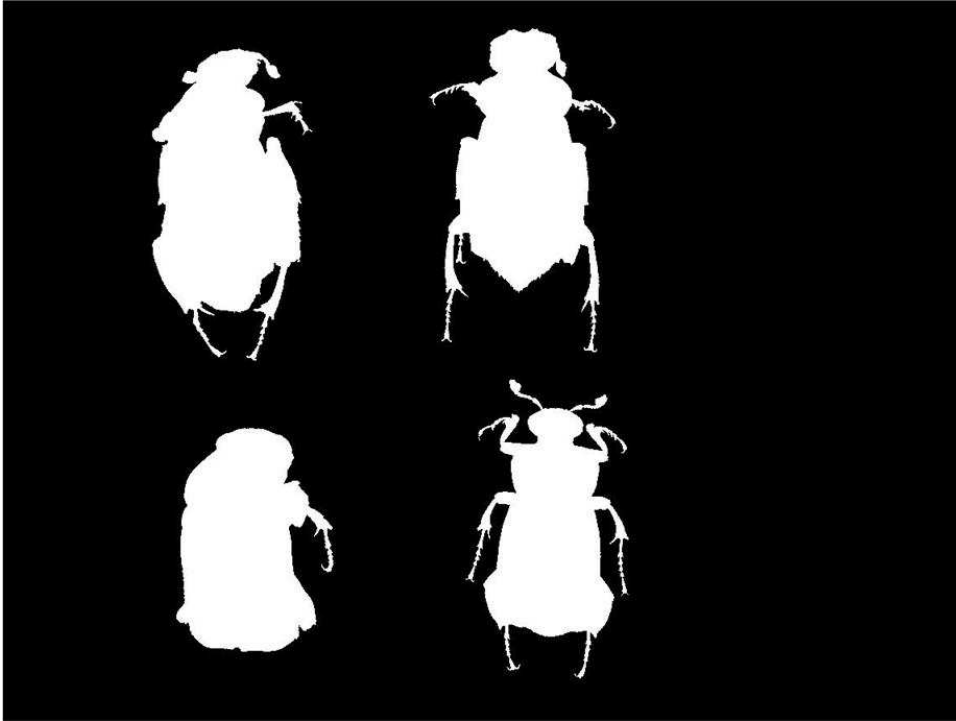
Figure 3.3: Representative binary image of insect specimens after morphological operations.

The morphological operations used to convert the initial JPEG color image to a binary image (Figure 3.3) unavoidably change each insect's shape however this generally has a minor effect on the final classification result. After the implementation of morphological operations to clean up the images, the next step is to extract an image of each insect separately to be used as training and validation images for classification operations. The first step to extract the shape of each insect is to label the connected components. A pixel $p(x, y)$ in the image, but not in the boundary, has two horizontal and two vertical neighbors constituting the set of 4 nearest neighbors (Figure 3.4(a)). The set of 4 nearest neighbors plus the four diagonal neighbors constitute the set of 8 nearest neighbors (Figure 3.4(b)).
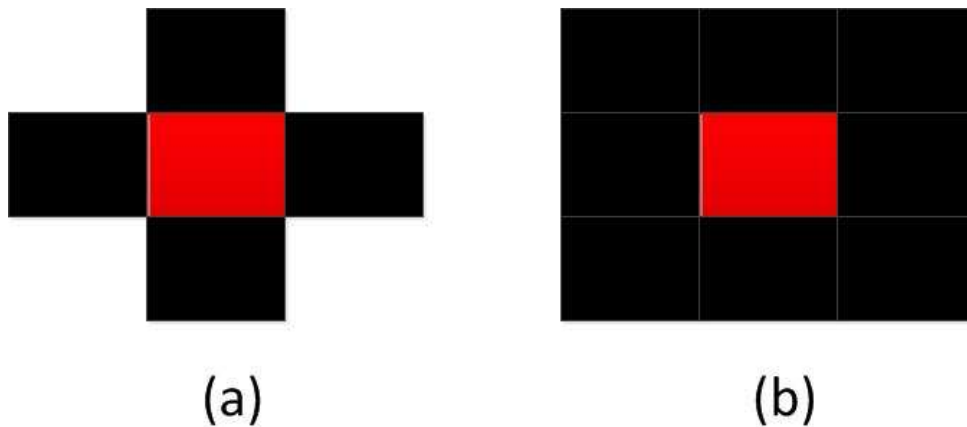
Figure 3.4: A pixel, represented by a red square, and its (a) 4 nearest neighbors; or (b) 8 nearest neighbors represented by black squares.

From the definitions of 4 and 8 nearest neighbors, two sets of foreground pixels, p and q, are defined as 4-connected or 8-connected when there is a 4-connected path or 8-connected path between them respectively. For an arbitrary foreground pixel p in the image, all foreground pixels which connect to it constitute an individual connected component [23].

Thus in the morphologically processed binary image, one insect body shape should only correspond to one connected component either in a 4-connected or 8-connected way. Furthermore, noise pixels in the background may constitute other connective components. A length filter is used to eliminate these redundant components ensuring the segmentation results only contain separate individual insect body shapes (Figure 3.5) which can eventually be used for classification. Binary images used in this classification work were on the order around 500 by 1000 pixels with some variations.
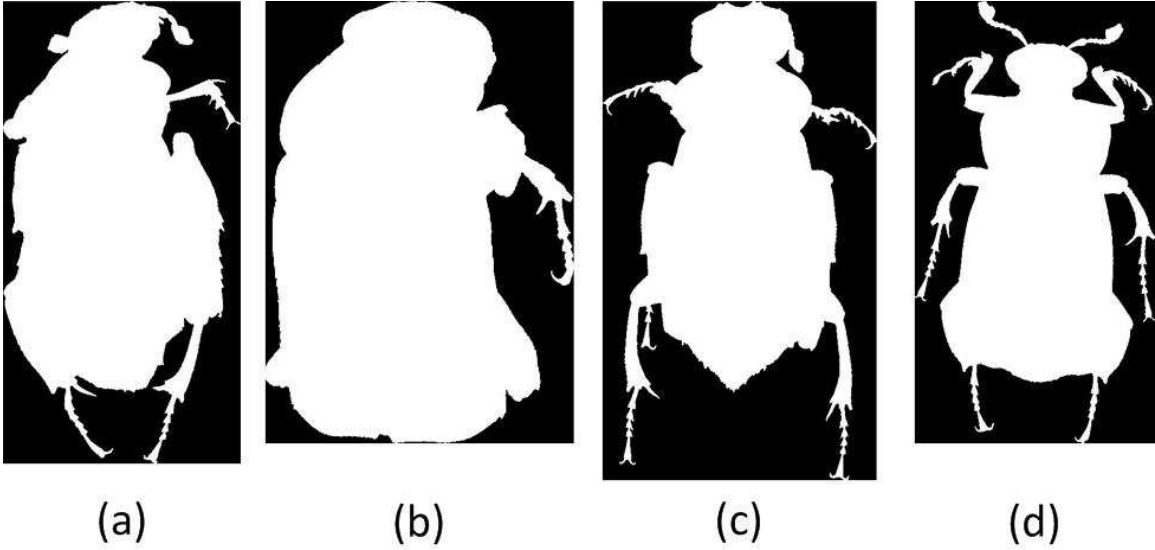
Figure 3.5: Representative segmentation results for individual insect body shapes of four American Burying Beetle specimens.

3.1.2 Object Alignment

The pose of each insect after segmentation will have some influence on ensuing shape analysis. In the segmented binary image, each pixel is presented by a two dimensional coordinate, (x, y), which distribute the foreground pixels along two axes called the main axis and auxiliary axis. Using a covariance matrix to analyze all object pixels in the insect body shape, it is expected that the two dimensional distribution of the pixels are not independent to each other. By using the proper projection of the data, it is desirable to have the two dimensional data with the least relevance as well as most energy preservation in each dimension separately.

The covariance matrix of each insect body shape can be represented as a 2 by 2 matrix:

$$C = \begin{pmatrix} C11 & C12 \\ C21 & C22 \end{pmatrix} \tag{3.2}$$

The eigenvectors of the covariance matrix can also be represented as a 2 by 2 matrix with each column containing an eigenvector:

$$V = \begin{pmatrix} V11 & V12 \\ V21 & V22 \end{pmatrix} \tag{3.3}$$

The rotation angle is calculated by:

$$\theta = \tan^{-1}(\frac{V11}{V21}) \tag{3.4}$$

After rotating the original image (Figure 3.6(a)) by the angle θ, the main axis and auxiliary axis of each insect shape are parallel to the new coordinate axis (Figure 3.6(b)). After rotation however, the insect head may be at the bottom and the abdomen at the top of the image (Figure 3.6(b)). For most insect species, the total number of object pixels in the abdomen is greater than in the head section. To account for this, first the image is divided into two equal segments along the vertical axis (Figure 3.6(c)). After which the object pixels within each segment are summed, if the top half of the image has more object pixels than the bottom half, the image is rotated 180 degrees prior to further use in classification (Figure 3.6(d)).

(a)   (b)   (c)   (d)
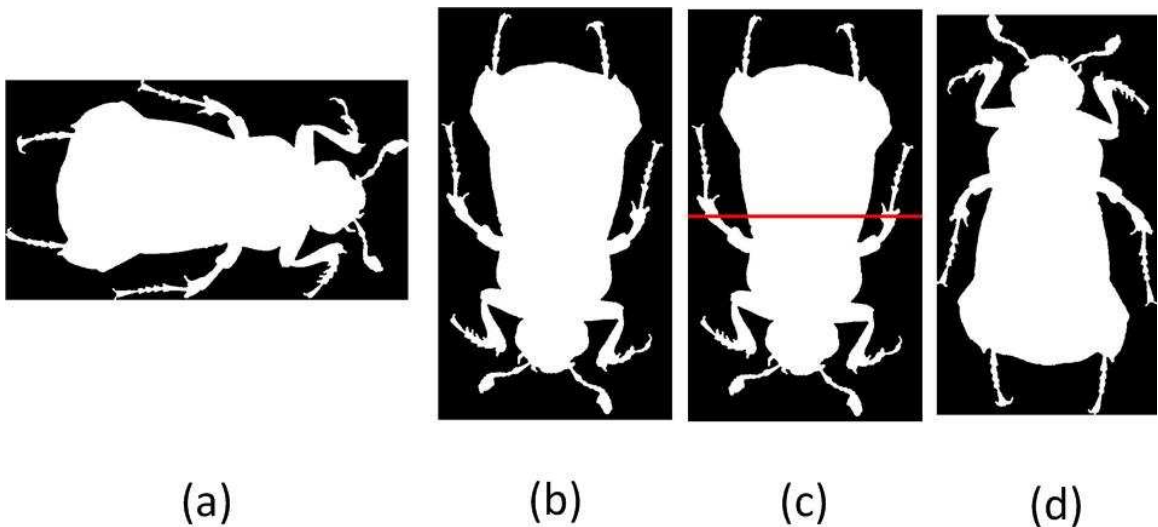
Figure 3.6: Steps in rotating a representative insect image (a) Original segmented image; (b) figure after rotation using eigenvectors with head at bottom; (c) image divided into top and bottom halves; (d) final rotated image with head at top.

3.1.3 Algorithm Flow

In summary, the processing of insect images starts with a color image. This is converted to a binary image followed by morphological operations to clean up the image prior to segmentation into connected components. Finally, these individual components are composed for subsequent classification tasks by orienting them about the central axis of the insect with the head at the top of the image (Figure 3.7).
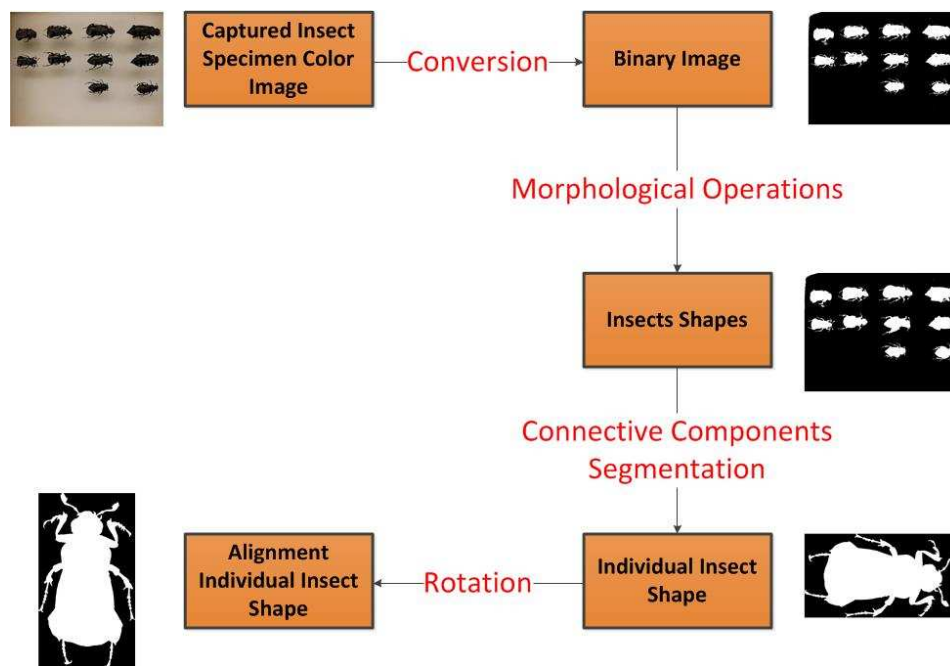
Figure 3.7: Algorithm flow of insect image preprocessing.

3.2 Region-based Shape Representation

Shape representation methods can generally be classified into two categories: region-based methods and contour-based methods. In region-based shape representation methods, as its name

suggests, shape features are extracted from the whole shape region [19]. Several classical region-based methods have been documented in recent decades. A set of second and third order 2-D moment invariants are widely used as the regional descriptor for its insensitivity to translation, scaling and rotation [23]. Zernike moments, which are the magnitudes of a set of orthogonal complex moments of an image, is the classical method for invariant image recognition [24]. With shape division methods, one or more basic region parameters are described in each sub-region area. These are then combined into an overall shape descriptor vector representing the overall region [27]. Based on string edit distance computation, string matching methods can be applied to 2-D shape recognition [26]. A novel grid string shape representation method is well presented for content-based image retrieval by Lu et al.[41].

In this investigation, we started with 11 different insect species with a total 92 images, which were obtained from the Oklahoma State University Entomology Museum collection and represent insect species typically captured in ABB traps (Table 1.1). Our first method for insect classification, called region-based shape representation, is described as follows: First, each binary image is divided into N equal area components along the vertical axis (Figure 3.8(b)).
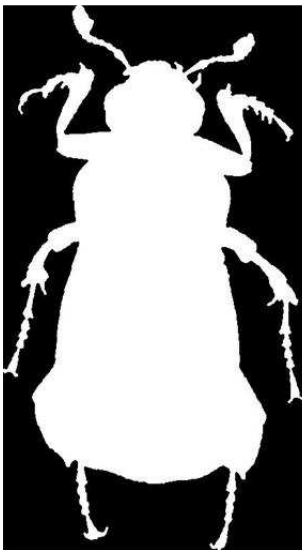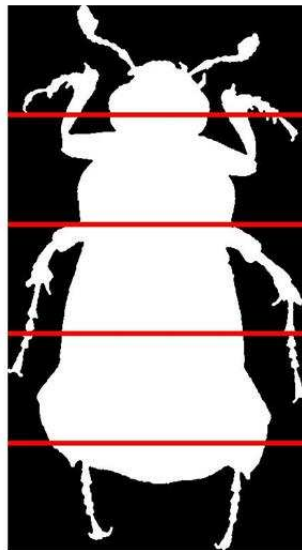
(a)   (b)

Figure 3.8: Representative insect image (a) after preprocessing image; (b) showing $N = 5$ area region-based classification representation.

The feature vector K (Eqn. 3.5) is then calculated by finding the K_i (Eqn. 3.6) for each of N area components in the binary insect shape.

$$K = (K_1, K_2, \dots, K_N)^T \tag{3.5}$$

$$\text{where } K_i = \frac{\#S_i}{\Delta S} \tag{3.6}$$

Where $\#S_i$ represents the number of object pixels in the ith area and ΔS represents the number of object pixels in the total insect shape.

The feature vector K represents the area proportions of the antennae, head, thorax and abdominal regions and provides a numerical representation of the general insect shape. In the training process, the feature vectors for all of the images of each species of insect are determined and then the mean of the individual vectors is calculated to represent a specific species. Unidentified images of insects are then classified to species by finding the minimum Euclidean distance between the new image feature vector and the mean feature vector of all the species. Classification accuracy, defined as the percentage of correctly identified images, was determined for each of the 11 species.

3.3 Experimental Results and Analysis of Region-based Shape Classification

Classification accuracy for each of the 11 species using the intuitive region-based shape representation method ranged from 0 to 100% for individual species. As the number of area components increased, classification accuracy for each species increased monotonically as did overall classification accuracy (Table 3.1).

Areas	S1	S2	S3	S4	S5	S6	S7	S8	S9	S10	S11	Overall
50	50%	56%	30%	30%	0%	83%	30%	50%	67%	50%	88%	48%
100	50%	56%	30%	40%	0%	83%	30%	50%	67%	50%	88%	49%
300	60%	56%	40%	60%	50%	83%	40%	50%	78%	88%	100%	64%

Table 3.1: Classification accuracy of 11 insect species (N=92) using different numbers of area components. S1 represents the American Burying Beetle (ABB).

By increasing area components in each insect shape image, the feature vector captures more details along the insect's body and higher accuracy is expected. However, with high dimensional features it is easy to get interference from noise. Principal component analysis (PCA) is an effective way to obtain dimension reduction while preserving the most important relationships within the data. When the region-based shape classification data was subjected to PCA analysis to reduce the dimensionality by a factor of between 3 and 15, the classification accuracy of individual species generally increased or stayed the same even with lower feature space dimension. Only in the case of species 3, for 20 principal area region classification, did the classification accuracy decline from 30% to 20%. Overall classification accuracy of the 20 and 50 principal area regions increased 11% and 13% respectively, while 100 principal area results were unchanged (Table3.2).

Areas	PCA dimen.	S1	S2	S3	S4	S5	S6	S7	S8	S9	S10	S11	Overall
300	20	60%	56%	20%	50%	33%	83%	40%	50%	78%	75%	100%	59%
300	50	60%	56%	30%	60%	33%	83%	40%	50%	78%	88%	100%	62%
300	100	60%	56%	40%	60%	50%	83%	40%	50%	78%	88%	100%	64%

Table 3.2: Classification accuracy of 11 insect species (N=92) for area components method using PCA. S1 represents the American Burying Beetle (ABB).

From the results above, it is obvious that using this intuitive region-based shape representation method does not result in sufficient classification accuracy of both ABB and overall for the ultimate use of this work. Informal observations of the insect images suggest that the insect bodies are relatively stable for feature extraction. However, the legs and antennae of the insects

are highly variable in pose among the different images. It was suspected that these factors would influence the precision of the region-based feature training process and decrease classification accuracy.

To verify this hypothesis, legs and antennae were manually removed from all of the segmented insect shapes (Figure 3.9) and the resulting new images subjected to the region-based shape classification methods, including the PCA dimension reduction.
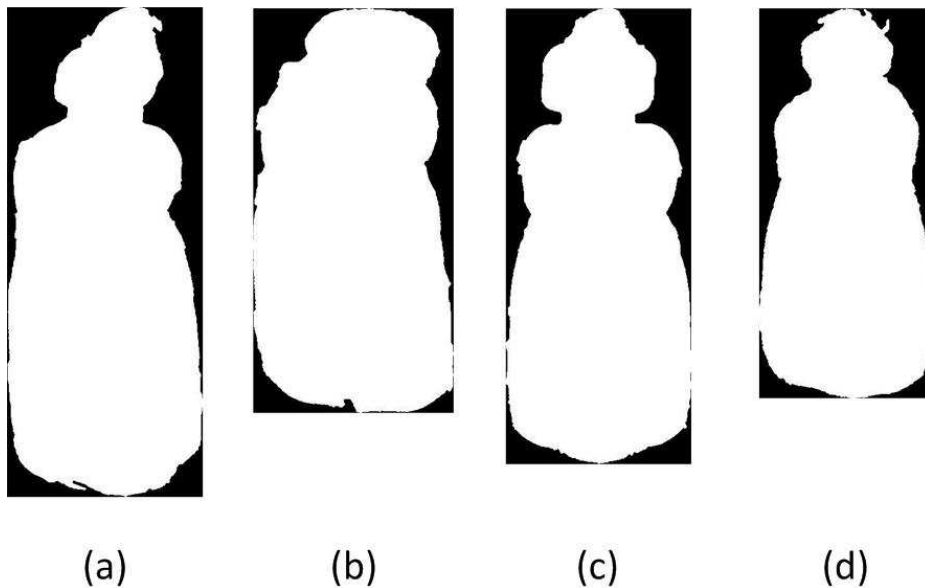
Figure 3.9: Binary images of four representative ABB specimens after manually removing legs and antennae.

Overall classification accuracy of the 11 species increased between 8 and 14% when using the images without legs and antennae. The change in classification accuracy for individual species ranged from an increase of 50% to decrease of 16% (Table 3.1 and Table 3.3).

Areas	S1	S2	S3	S4	S5	S6	S7	S8	S9	S10	S11	Overall
50	50%	78%	50%	40%	17%	67%	20%	67%	89%	75%	88%	58%
100	60%	78%	50%	40%	17%	67%	40%	67%	89%	100%	88%	63%
300	60%	78%	70%	50%	50%	83%	50%	67%	100%	100%	88%	72%

Table 3.3: Classification accuracy of 11 insect species (N=92) for area components method on images with legs and antennae manually removed.

Subjecting the data from images of insects with manually removed legs and antennae to PCA analysis further increased overall classification accuracy of principal 20 and 50 area region results by 6% and 5% respectively (Table 3.3 and Table 3.4).

Areas	PCA dimen.	S1	S2	S3	S4	S5	S6	S7	S8	S9	S10	S11	Overall
300	20	60%	78%	50%	40%	17%	83%	20%	67%	100%	100%	88%	64%
300	50	60%	78%	70%	50%	17%	83%	40%	67%	100%	100%	88%	68%
300	100	60%	78%	70%	50%	50%	83%	50%	67%	100%	100%	88%	72%

Table 3.4: Classification accuracy of 11 insect species (N=92) for area components method using PCA on images with legs and antennae manually removed.

From these results, the classification accuracies for both methods have been dramatically enhanced by analyzing images without legs or antennae. It can be concluded that shape uncertainty introduced by leg and antenna features will influence shape feature analysis as well as decrease classification accuracy. For this reason automatic removal of legs and antennae from insect shapes is a necessary procedure which is discussed in Chapter 4.

CHAPTER IV

CONTOUR-BASED SHAPE REPRESENTATION

In contrast to region-based shape representation methods, contour-based shape representation methods use contour shape features for classification. Furthermore, contour-based shape representation methods are generally classified into continuous and discrete approaches. A continuous approach tends to maintain boundary integrity without dividing a shape, while a discrete approach breaks the boundary of the shape into multiple segments [19]. For continuous contour-based shape representation methods, two spectral descriptors, the Fourier descriptor [11] and wavelet descriptor [42] have been proposed to reduce noise sensitivity and accommodate boundary variations. They have been widely used for shape representation and retrieval [30-33, 43-45]. For discrete contour-based shape representation methods, polygon curve decomposition [37], hidden Markov model-based shape descriptors [38] and shape contexts [35] were developed for shape matching and recognition.

In this chapter, Fourier descriptors are used for insect shape representation and classification. In previous classification efforts, the legs and antennae in insect images were found to have a negative influence on shape analysis and limited classification accuracy. To mitigate this shape uncertainty, a shape decomposition method based on visual curvature [1] was proposed and implemented to automatically remove legs and antennae from the insect images prior to subjecting them to classification using contour-based shape representation. The results of classification using both area component and Fourier descriptor methods are presented in detail

for the 11 species of insects (N=92) that were used in the previous analysis.

4.1 Fourier Descriptor of a Closed Contour

The Fourier coefficients of a shape's chain encoded contour was first proposed as a spectral descriptor by Kuhl and Giardina [11] in order to overcome boundary variations and noise sensitivity [19]. This is one of the most widely used shape descriptor methods and is discussed by numerous papers [43, 45]. The Fourier descriptor is a kind of shape signature that uses a one-dimensional function to describe the boundary line of a two-dimensional object [32].

4.1.1 Fourier Descriptor from DFT of Closed Insect Shape

The shape boundary extracted from the preprocessed insect body shape is a closed curve that can be represented by a set of coordinates $(x_i, y_i), i = 1, 2, ..., L$ where L is the number of boundary points. By representing the x, y plane in complex notation, every boundary point can be presented as $Z = x + jy$. For the L boundary points, the boundary line could be described as a complex sequence $Z(n), n = 0, 1, ..., L - 1$. Any periodic signal of finite length can be expressed in terms of complex exponentials, thus the contour of an insect body shape can be transformed by applying the discrete Fourier transform (DFT) to the complex sequence of the insect shape [32]. If the results of the DFT are labeled as $F(n), n = 0, 1, ..., L - 1$, this Fourier descriptor preserves all of the boundary information (Eqn. 4.1).

$$F(n) = \frac{1}{L} \sum_{i=0}^{L-1} Z(n) \exp\left(\frac{-j2\pi ni}{L}\right) \; n = 0, 1, ..., L - 1 \qquad (4.1)$$

4.1.2 Fourier Descriptor Normalization

Fourier descriptors preserve all of the boundary information, including shape position, direction and scale. However, a change in any of these factors will affect all of the Fourier descriptors. For shape representation and retrieval, the shape descriptor should only describe the shape itself and

be unaffected by the other factors. For that reason, Fourier descriptors need to be normalized to satisfy the objective of translational, rotational and scale invariance.

The centroid distance, r_i, is defined as the distance of the boundary points from the centroid (x_c, y_c) of the shape (Eqn. 4.2).

$$r_i = ([x_i - x_c]^2 + [y_i - y_c]^2)^{1/2}, i = 1, 2, \ldots, L \tag{4.2}$$

Where (x_c, y_c) are the average of the x coordinates and y coordinates of the boundary shape respectively [46]. In the DFT, the boundary is normalized to N which is the integer power of 2.

$$f_n = \frac{1}{N} \sum_{i=0}^{N-1} r_i \exp\left(\frac{-j2\pi ni}{N}\right) n = 0, 1, \ldots, N-1 \tag{4.3}$$

The coefficients $f_n, n = 0, 1, \ldots, N-1$ are defined as the Fourier descriptors of the shape (FD), denoted as $FD_n, n = 0, 1, \ldots, N-1$ respectively.

The Fourier descriptors based on the centroid distance are translation invariant. To achieve rotation invariance, only magnitude information $|FD_n|$ without phase information is preserved. In addition, scale invariance is implemented by dividing the magnitudes of the DC components, denoted as $|FD_0|$. Finally, the feature vector used as the Fourier descriptor describing the shape is presented by equation 4.4:

$$f = \left[\frac{|FD_1|}{|FD_0|}, \frac{|FD_2|}{|FD_0|}, \ldots, \frac{|FD_N|}{|FD_0|}\right]^T \tag{4.4}$$

In the Fourier descriptors, the low-frequency coefficients preserve the primary shape information of the boundary whereas the higher-frequency coefficients represent finer shape structures and noise. When this procedure is used as the object shape description method, only a subset of low-

frequency coefficients from the original Fourier descriptors are kept to retain the main shape information while getting rid of finer structures and noise.

4.1.3 Experimental Results and Analysis for Insect Classification

In the contour-based shape representation method, each insect body shape (Figure 4.1a) was first converted to the insect boundary (Figure 4.1b). This boundary was then subjected to DFT using distance to the centroid and finally the DFT coefficients were normalized.

(a)   (b)   (c)   (d)   (e)
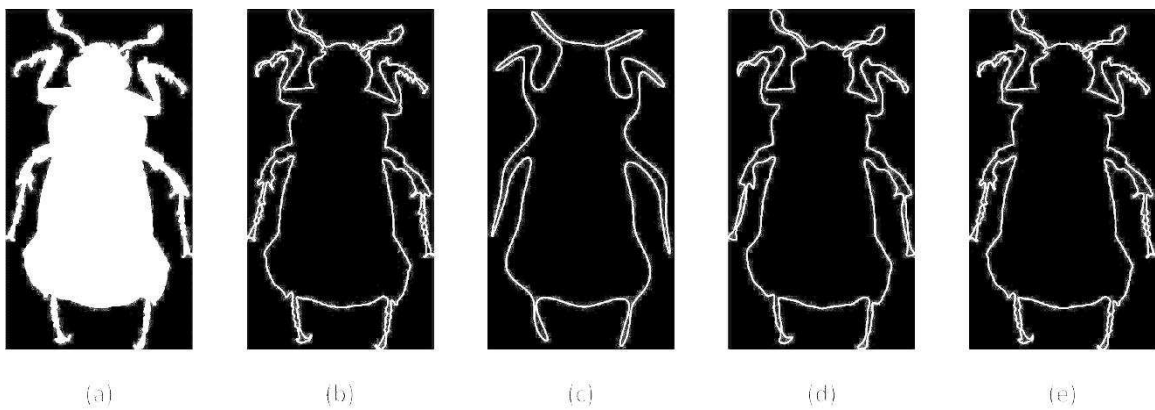
Figure 4.1: (a) Representative binary insect body shape and (b) insect boundary shape. Reconstructed insect boundary shapes using the lowest: (c) 64 DFT coefficients; (d) 256 DFT coefficients; (e) 1024 DFT coefficients.

To capture global features, the original Fourier descriptors were truncated to the N lowest frequency coefficients to represent the feature vector of each image. Even though a finer shape could be achieved using more DFT coefficients, such as 1024 DFT coefficients in figure 4.1(e), a high dimensional feature vector is very sensitive to noise or small distortions. As a trade-off in these experiments, N was set equal to 64, 128 and 256 coefficients. After feature extraction was performed on all images, each insect species was characterized by taking the mean of all of the feature vectors for that species. In the classification process, each image was then classified to

species by finding the smallest Euclidean distance between the unknown image feature vector and

the mean feature vectors of all 11 species.

Fourier coefficients	S1	S2	S3	S4	S5	S6	S7	S8	S9	S10	S11	Overall
64	30%	67%	30%	50%	50%	67%	20%	33%	89%	100%	63%	54%
128	30%	67%	30%	50%	50%	67%	20%	50%	89%	100%	63%	56%
256	30%	67%	30%	50%	67%	67%	20%	50%	89%	100%	63%	57%

Table 4.1: Classification accuracy on preprocessed shape images of 11 species of insects (N=92) using Fourier descriptor method for 64, 128 and 256 Fourier coefficients. S1 is ABB.

As the number of frequency coefficients increases, the overall classification accuracy increased

only slightly from 54% to 57% (Table 4.1). ABB classification accuracy is 30% for all feature

vector lengths. ABB and overall classification accuracies using this method are not satisfactory

due to shape uncertainty introduced by the legs and antennae of the insect subjects. To verify this

observation, legs and antennae were removed manually from the binary shape images and the

classification algorithm using Fourier descriptors was repeated. Classification accuracies of all

individual species, except S4 and S10, increased. Overall classification accuracy increased from

54-57% to 78% and was unaffected when the number of Fourier coefficients was varied between

64 and 256. Classification accuracies of S5, S6, S9 and S10 reached 100% (Table 4.2).

Based on the results obtained (Table 4.1 and 4.2), 256 DFT coefficients was selected for use in

ensuing experiments.

Fourier coefficients	S1	S2	S3	S4	S5	S6	S7	S8	S9	S10	S11	Overall
64	80%	89%	40%	50%	100%	100%	60%	67%	100%	100%	75%	78%
128	80%	89%	40%	50%	100%	100%	60%	67%	100%	100%	75%	78%
256	80%	89%	40%	50%	100%	100%	60%	67%	100%	100%	75%	78%

Table 4.2: Classification accuracy on manually decomposed shape images of 11 species of insects (N=92) using Fourier descriptor method for 64, 128 and 256 Fourier coefficients. S1 is ABB.

Compared to the area component method, the Fourier descriptor method is more sensitive to shape uncertainty and resulted in improved classification accuracy. Classification accuracy of both methods was improved by removing variability that arose from uncertainly in the pose of legs and antennae. For that reason we present a curvature-based approach to automatically remove legs and antennae from insect images in order to improve classification accuracy.

4.2 Visual Curvature [1]

In order to remove legs and antennas precisely from an image of an insect, the most important task is to identify the locations where legs and/or antennae are connected to the body (Figure 4.2).
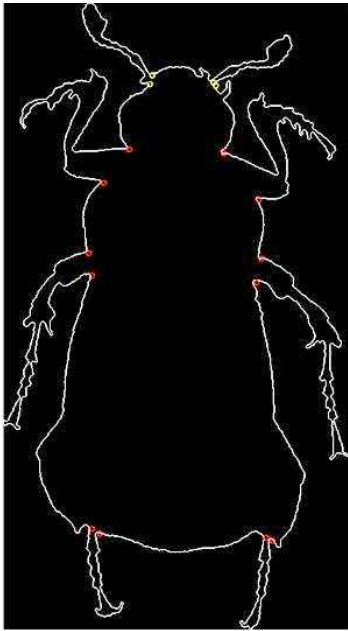
Figure 4.2: Insect shape boundary with yellow and red dots indicating antenna-body and leg-body connection points respectively.

The task of locating the connections described above can be classified as a corner detection problem. Corners are critical features used in describing objects and are essential for pattern recognition [47]. Various corner detection methods based on curvature have been proposed previously [47-51]. Due to distortion from noise and varying levels of detail in images, the

desired curvature should reflect contour information at different scales, be unaffected by noise, invariant under rotation and translation, as well as be suitable for smooth curves and polygonal arcs [1].

In this investigation visual curvature, proposed by Liu et al [1], is implemented to locate the candidate connection points as the starting point to remove unnecessary shape distractors. Visual curvature is based on statistics of the extreme points of the height function computed over all directions which combine regular curve features in the geometry and turn angle information of polygonal curves together. The complete visual curvature algorithm is organized as follows:

- Step 1: After getting the insect shape boundary, every boundary point is assigned to a coordinate in the original coordinate system (Figure 4.3).
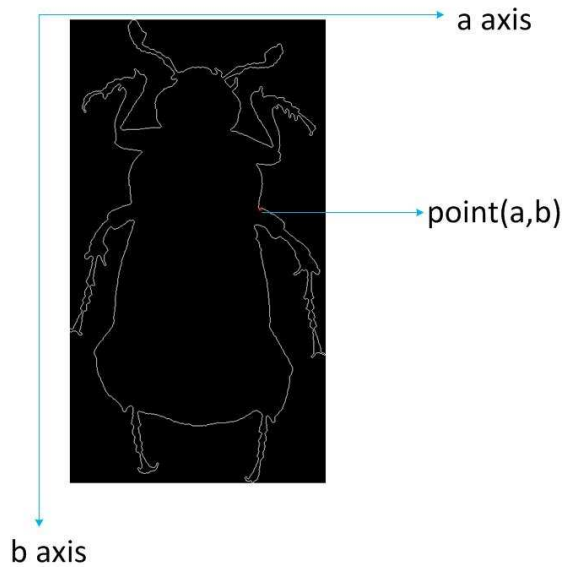
Figure 4.3: Boundary point coordinate in the original coordinate system.

- Step 2: The contour is parameterized by the distance from each point to the b-axis, denoted by $x(s)$. At first, the parameter for each point is its b coordinate. By rotating the coordinate system by angle α anticlockwise, $\alpha_i = \pi \frac{i}{N}, i = 0, ..., N - 1$, we obtain a

series of height functions H_{α_i}, where each height function H_{α_i} presents all boundary point parameters in the α_i direction.

$$x(s) = a\cos\alpha_i + b\sin\alpha_i, \alpha_i = \pi\frac{i}{N}, i = 0, 1, \dots, N - 1 \tag{4.5}$$

- Step 3: For a point on the curve C, suppose $S(v)$ is its neighborhood of size ΔS on the curve C, the visual curvature of point v is defined as:

$$K_{N,\Delta S}(v) = \pi\frac{\sum_{i=0}^{N-1}\#[H_{\alpha_i}(S(v))]}{N\Delta S} \tag{4.6}$$

Where $\#[H_{\alpha_i}(S(v))]$ represents the local extreme points of the height function H_{α_i} in the neighborhood $S(v)$. As mathematically defined above, each boundary point's visual curvature is estimated by its small neighborhood $S(v)$. For every height function, the extreme points are identified and those that are in this neighborhood are counted. After summing up all the numbers in all directions, each point's visual curvature is calculated using equation 4.6. In the current implementation, setting $\Delta S = 1$, yields the most robust curvature estimation for digital contours.

- Step 4: From the definition of visual curvature above, all extreme points are counted without considering whether they are important or not. In fact, at certain scales small concave or convex segments should be ignored and only relatively important extreme points should be calculated. Using this algorithm, the multi-scale visual curvature of the point v is defined to be:

$$K_{N,\Delta S}(v) = \pi\frac{\sum_{i=0}^{N-1}\#[H_{\alpha_i}^{\varepsilon}(S(v))]}{N\Delta S} \tag{4.7}$$

In this expression, ε is a scale factor and $\#[H_{\alpha_i}^{\varepsilon}(S(v))]$ represents the number of the extreme points of the height function H_{α_i} in the neighborhood $S(v)$ whose scale measure is not smaller than ε.

33

- Step 5: The scale measure of an extreme point v in the height function H_α is denoted by $\varepsilon_\alpha(v)$:

$$\varepsilon_\alpha(v) = \frac{r_\alpha(v)}{h_\alpha} \tag{4.8}$$

The height H_α denoted by h_α is the absolute difference between the maximum and minimum values in the height function H_α. Furthermore, the scale measurement of a local extreme point v in the height function H_α, denoted by $r_\alpha(v)$, is presented in Figure 4.4 and equations 4.9 through 4.11.
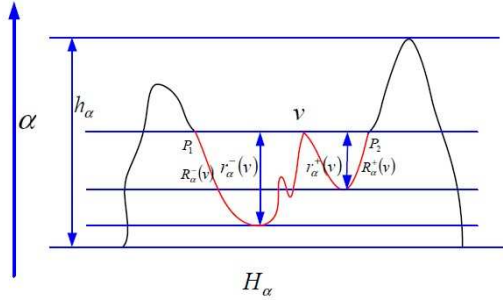
Figure 4.4: The scale measure of an extreme point v in the height function H_α [1].

For a local extreme point v in the height function H_α, its influence region $R_\alpha(v)$ is defined by the maximal neighborhood such that the height of every point in this neighborhood is not greater (lower) than the height of the point v. For example, the influence region for local maximum point v in Figure 4.4 is the red curve from point P_1 to P_2. If the point v is not an absolute extreme value, $R_\alpha(v)$ is divided into two segments by v, the left segment $R_\alpha^-(v)$ and the right segment $R_\alpha^+(v)$.

$$r_\alpha(v) = \min[r_\alpha^+(v), r_\alpha^-(v)] \tag{4.9}$$

$$r_\alpha^+(v) = \max\{|H_\alpha(p) - H_\alpha(v)| \,|\, p \in R_\alpha^+(v)\} \tag{4.10}$$

$$r_\alpha^-(v) = \max\{|H_\alpha(p) - H_\alpha(v)| \,|\, p \in R_\alpha^-(v)\} \qquad (4.11)$$

As denoted above, $r_\alpha^+(v)$ and $r_\alpha^-(v)$ are the maximal height differences between point v and the points belonging to $R_\alpha^+(v)$ and $R_\alpha^-(v)$, respectively. Equation 4.8 computes the scale for each local extreme point in the height function. The importance of the local extrema depends not only on the height of this point, but also on the scale of the contour.

For a point on the contour in each height function, if it is the local extreme point, it is counted when the scale measure is larger than the threshold ε. The visual curvature for each boundary point is calculated by equation 4.7 using the same scale ϵ.

- Step 6: Because of digitalization, some high curvature points may disappear since the curvature is spread to several adjacent points as illustrated in Figure 4.5. The curvature at point O is not represented by a pixel at that location but represented by the sum of the curvature of adjacent points.
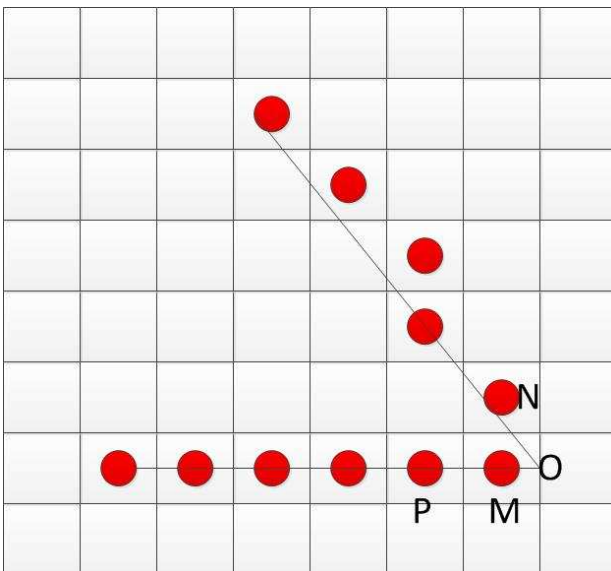
Figure 4.5: Example of a high curvature point disappearing due to digitalization [1].

In the current implementation, after calculating the visual curvature for all boundary points, they are ranked from high to low monotonically. The point v with highest visual curvature is selected and the visual curvatures of adjacent points are added to it within its neighborhood $U(v)$ of radius T (Eqn. 4.12).

$$DK^{\varepsilon}_{N,\Delta S}(v) = \sum_{u \in U(v)} K^{\varepsilon}_{N,\Delta S}(u) \tag{4.12}$$

At the same time, the digital visual curvature of all other points in the neighborhood are set to zero. Except for these recalculated points, this is repeated for the second largest visual curvature point, then the third, and so on. The algorithm ends when there is no change in the visual curvature presentation of all boundary points.

In the algorithm described above, several parameters need to be tuned to yield the best results. For these experiments, N=128, ΔS=1 and T=10 and the visual curvature can be rewritten as:

$$K(v) = \sum_{i=0}^{N-1} \#[H^{\epsilon}_{\alpha_i}(S(v))] \tag{4.13}$$

Two parameters in Equation 4.13 will affect the results of whether a boundary point is selected as a candidate connection point. The first parameter is the scale threshold, denoted as ε and the second is the threshold of visual curvature K. To find the best choice of parameter K, several experiments based on different K values were conducted. According to human perception, $K = 10$ preserved all the important candidate points and it produced a relatively small candidate point set. Also, the average number of candidate connection points decreased from 57 to 48 on the 92 images used in this study when ε was changed from 0.010 to 0.015.
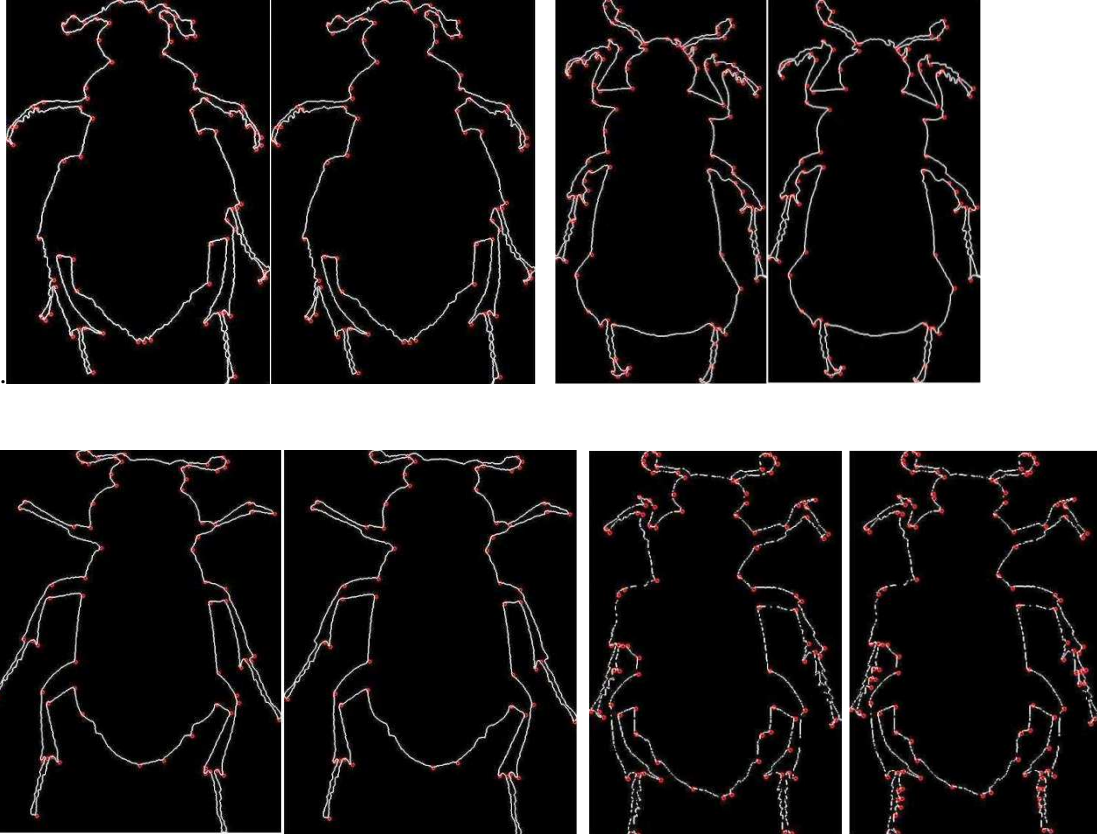
Figure 4.6: Representative images of 4 insects subject to visual curvature algorithm (K=10) with scale threshold ε=0.010 left image, and ε=0.015 right image. Red dots indicate the boundary points where visual curvature is larger than visual curvature and scale threshold.

Compared to the ideal leg and antennae connection points (Figure 4.2), the visual curvature algorithm yields more candidate connection points which makes selecting cutting points more complicated. A smaller scale threshold ϵ results in the detection of more candidate points on the contour. This is more likely to preserve the real joint points on the contour, which is helpful for further processing. On the other hand, if numerous redundant candidate points are detected in addition to the real joint points, it will make the cutting algorithm more complicated and time-consuming. Thus a proper scale threshold ε is significant not only for visual curvature but also shape decomposition results.

In subsequent discussions on this chapter, both sets of parameters, $\varepsilon=0.010$ and $K=10$ as well as $\varepsilon=0.015$ and $K=10$, are used for visual curvature implementation and candidate connection point selection for future shape decomposition.

4.3 Visual Curvature Based Shape Decomposition

After the visual curvature algorithm identifies candidate connection points on each insect image (Figure 4.6) these can be used to cut legs and antennae using shape decomposition techniques to reduce uncertainty in classification.

Shape decomposition methods using convexity and concavity rules have been thoroughly documented [5-8] however these techniques have not, to the best of our knowledge, been applied specifically to insect classification tasks. Based on observable insect characteristics, an intuitive insect shape decomposition algorithm was proposed. Throughout the following presentation American Burying Beetle image #2 (Figure 4.7a) will be used to illustrate the algorithm progression. The visual curvature parameters of $\varepsilon=0.015$ and $K=10$ are used in the algorithm to identify candidate connection points (Figure 4.7c) from the boundary shape (Figure 4.7b). Final cuts to separate legs and antennae from the body shape are made among the pairs of points contained in the set of candidate connection points.
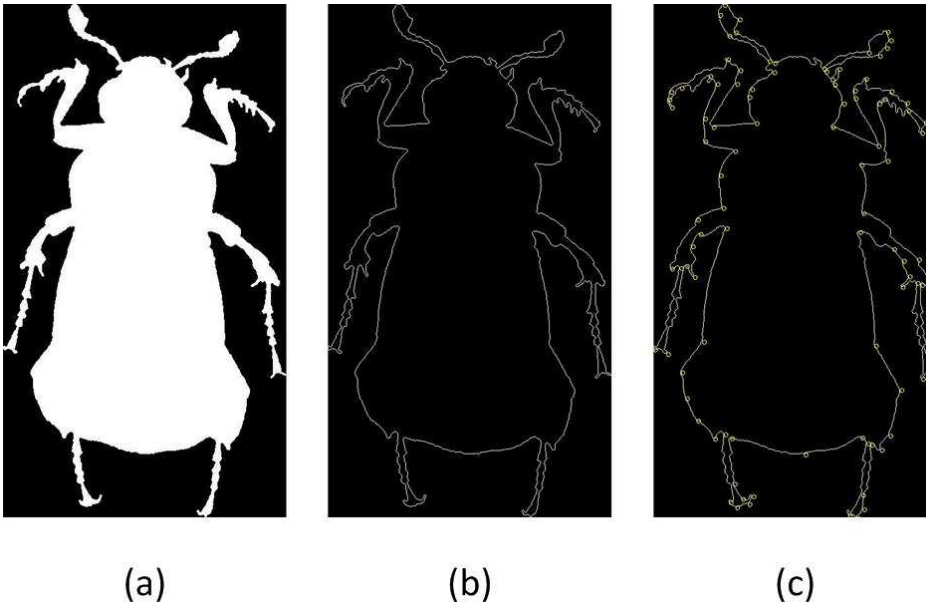
Figure 4.7: (a) Original image; (b) boundary shape; (c) candidate connection points identified by visual curvature algorithm in ABB specimen 2.

The Visual Curvature Based Shape Decomposition algorithm consists of the following steps:

- Step 1: First the image is divided into two segments defined by the center line of the image along the horizontal direction (Figure 4.8b). Due to morphology of the insects of interest, this will place the pairs of candidate connection points, along which the final cut to separate the leg or antenna is made, in the same image segment. Each segment will be treated separately and cutting lines will be determined among candidate connection points independently in each side. This algorithm arbitrarily treats the left segment first followed by the right segment.
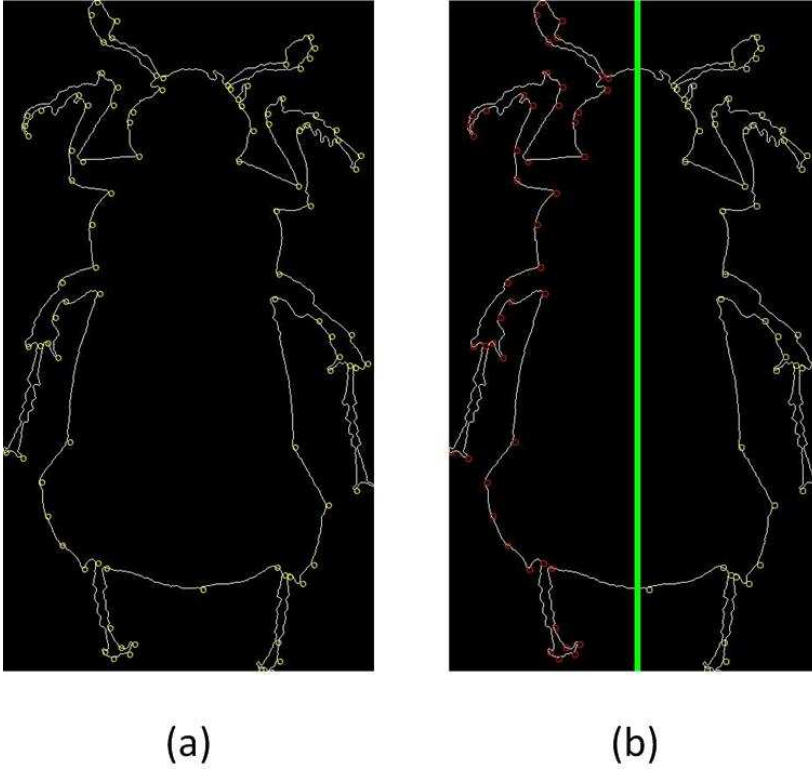
Figure 4.8: (a) Visual curvature result on boundary shape; (b) left and right segment on shape.

- Step 2: Each side of the image has several candidate connection points (Figure 4.8b). Assume that there are m points in the left side and n points in the right side. Theoretically, each pair of candidate connection points could make one possible cut. That is, there are $m(m-1)/2$ possible candidate cuts in the left side and $n(n-1)/2$ possible candidate cuts in the right side.
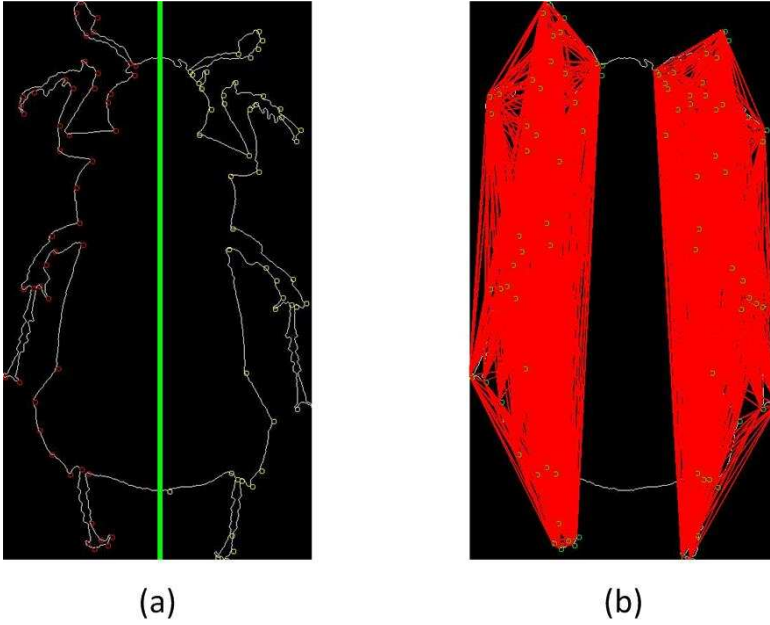
Figure 4.9: (a) Left and right segment of shape; (b) all possible candidate cuts in each side from pairs of candidate connection points.

The objective of this insect shape decomposition algorithm is to find the cuts which precisely separate legs and antenna among the candidate cuts in each side that mimic what human vision can discern (Figure 4.10).
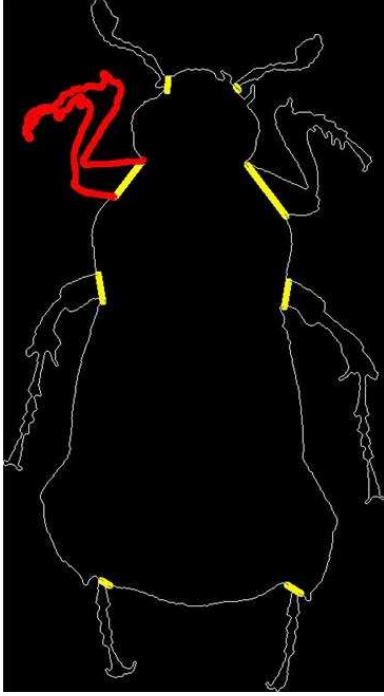
Figure 4.10: Ideal cutting lines for legs and antennae identified by human vision. Yellow lines represent cutting lines and red lines represent pixels along contour of one leg to be cut.

From careful observation of the ideal cutting lines there is a unique relationship between the two candidate connection points. If the shape contour is represented by a two dimensional coordinate sequence in a clockwise direction, we know the number of contour pixels between each pair of candidate connection points. This is called the pixel distance. Specifically for the upper left leg in Figure 4.10, the contour pixels are red in color. In addition, it is straight forward to calculate the Euclidean distance between these two candidate connection points as well. According to morphological characteristics of insect leg and antenna shapes, the distance ratio r determined by Equation 4.14 tends to be large when the two connecting points form a reasonable cut on the insect shape.

$$r = \frac{P_s}{E_s} \tag{4.14}$$

Where P_s denotes the pixel distance and E_s denotes the Euclidean distance of two candidate connection points. Candidate cuts are denoted by C, where L and R represent the left side and right side respectively. The C(L)= $m(m-1)/2$ possible candidate cuts on the left and C(R)= $n(n-1)/2$ possible candidate cuts on the right, are sorted by distance ratio r in descending order, respectively.

$$C(L) = \{cut_1 \ldots cut_{m(m-1)/2}\}, \qquad r_1 \geq r_2 \geq \cdots \geq r_{m(m-1)/2} \tag{4.15}$$

$$C(R) = \{cut_1 \ldots cut_{n(n-1)/2}\}, \qquad r_1 \gg r_2 \geq \cdots \geq r_{n(n-1)/2} \tag{4.16}$$

Because the distance ratio for reasonable cuts trends to be large, the candidate cut sets $C(L)$ and $C(R)$ may be truncated by setting a threshold γ:

$$C_\gamma(L) = \{cut_1 \ldots cut_p\}, \qquad r_1 \geq r_2 \geq \cdots \geq r_p \geq \gamma \tag{4.17}$$

$$C_\gamma(R) = \{cut_1 \ldots cut_q\}, \qquad r_1 \geq r_2 \geq \cdots \geq r_q \geq \gamma \tag{4.18}$$

A distance ratio threshold, and resulting truncated candidate cut sets, will be used to find the final reasonable cuts.

- Step 3: In addition to the distance ratio mentioned above, there are additional intrinsic characteristics for reasonable cuts in shape decomposition.
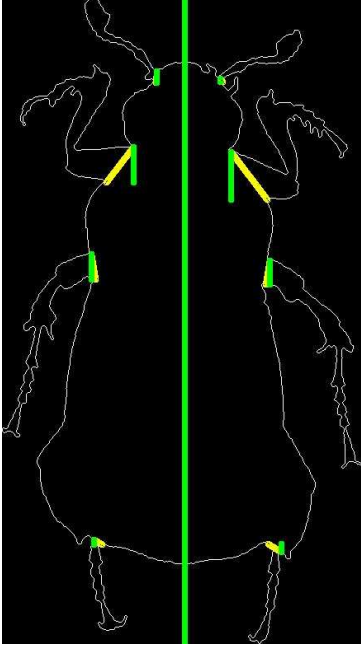
Figure 4.11: The example cutting line according to human vision using ratio of vertical distance in cut to total shape length.

The first characteristic of reasonable cuts is that they should be totally contained within the insect body. If the connection line between two candidate connection points is totally or partially outside the insect body shape, it should not be a reasonable and correct cut for separation. To check for this, U is set as the union of all pixels in the insect body shape and a binary value is assigned for each candidate cut_i:

$$a_{cut_i} = \begin{cases} 0 & cut_i \in U \\ 1 & cut_i \notin U \end{cases} \tag{4.19}$$

The candidate cut set satisfying this condition is expressed by:

$$C_a(L) = \{cut_1 \dots cut_p\}, \; a_{cut_1} = \cdots = a_{cut_p} = 0 \tag{4.20}$$

$$C_a(R) = \{cut_1 \dots cut_q\}, \; a_{cut_1} = \cdots = a_{cut_q} = 0 \tag{4.21}$$

Using this limitation, numerous candidate cuts can be removed which results in a new smaller candidate cut set (Figure 4.12b).

(a)　　　　　　　　　　(b)　　　　　　　　　　(c)
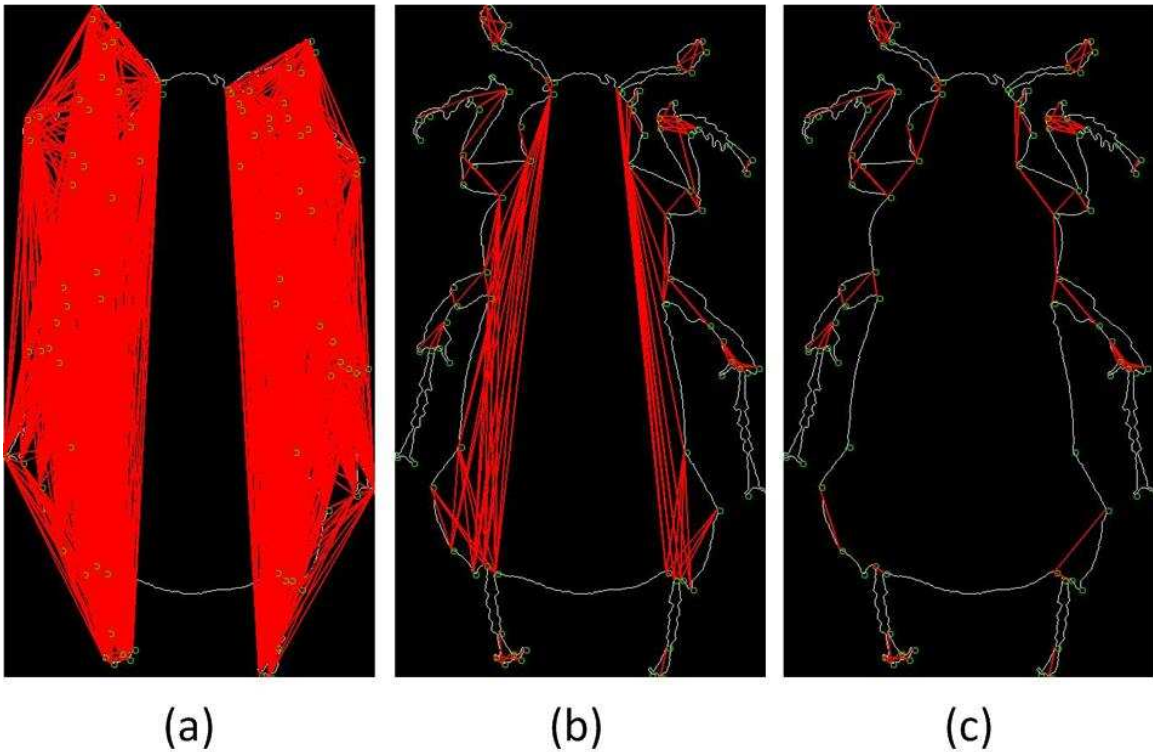
Figure 4.12: Representative insect body shape showing (a) all possible candidate cuts in each side, (b) possible candidate cuts contained in the body shape in each side after removing cuts that contain pixels outside the body shape and (c) possible candidate cuts contained in the body shape after applying length ratio threshold.

The second check for reasonable cuts concentrates on the difference between the vertical component of a candidate cut compared to the total shape length. In Figure 4.11 for each cut labeled by a yellow line, the vertical coordinate difference for two candidate connection points labeled as green line is not very large. In other words, the ratio between this difference and image vertical length, which is called the length ratio, should be relatively small. For each cut,

$$R = \frac{D}{D_I} \tag{4.22}$$

Where D denote the coordinate vertical difference between two points for the cut and D_I denote the image vertical length. Because the length ratio for a reasonable cut tends to be small, the candidate cut set $C(L)$ and $C(R)$ can be reduced by setting the threshold δ:

$$C_\delta(L) = \{cut_1 \dots cut_p\}, \qquad R_1 < \delta \text{ \& } R_2 < \delta \dots \text{\& } R_p < \delta \tag{4.23}$$

$$C_\delta(R) = \{cut_1 \dots cut_q\}, \qquad R_1 < \delta \text{ \& } R_2 < \delta \dots \text{\& } R_q < \delta \tag{4.24}$$

The third step is to combine the step that checks if the cut is within the body with the length ratio restriction to reduce the candidate cut list further. The result of this step when using a length ratio limitation with $\delta = 1/10$ is shown in Figure 4.12c. Additional candidate cuts are removed by combining the two procedures. These cuts represent a small subset (Eqn. 4.25 and 4.26) from the original candidate cuts.

$$C_{\delta,a}(L) = \{cut_1 \dots cut_p\}, \qquad R_1 < \delta \text{ \& } R_2 < \delta \dots \text{\& } R_p < \delta, a_{cut_1} = \dots = a_{cut_p} = 0 \tag{4.25}$$

$$C_{\delta,a}(R) = \{cut_1 \dots cut_q\}, \qquad R_1 < \delta \text{ \& } R_2 < \delta \dots \text{\& } R_q < \delta, a_{cut_1} = \dots = a_{cut_q} = 0 \tag{4.26}$$

- Step 4: After the candidate cut extraction, the new set of reasonable cuts compares well to the cuts identified by human vision (Figure 4.13).
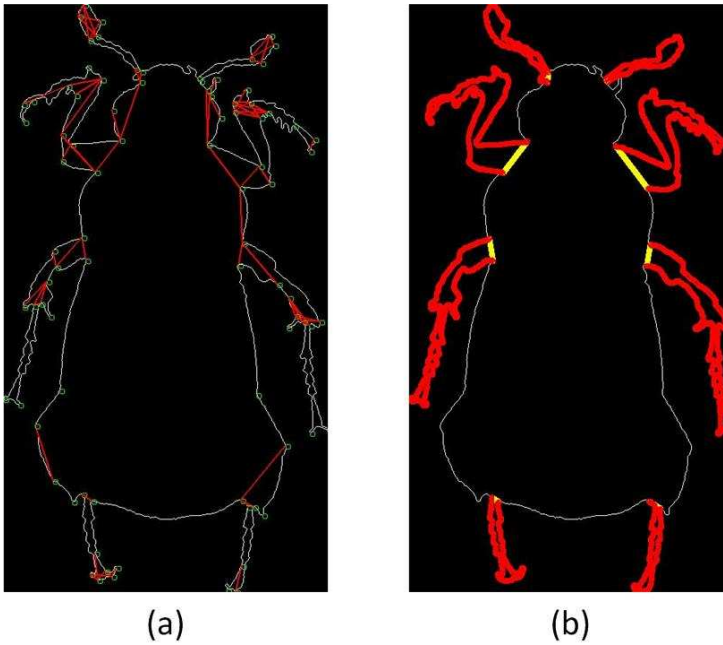
Figure 4.13: Representative image showing (a) possible candidate cuts contained in the body shape and subject to length ratio threshold; (b) the ideal cutting lines according to human vision.

As mentioned is step 2 above, the distance ratio r determined by pixel distance and Euclidean distance trends to be large when the two connection points are a reasonable cut on the insect shape. Due to the uncertain distribution of candidate connection points found by the visual curvature algorithm, it is not possible to conclude that the connection with highest distance ratio is the reasonable cut. However, as illustrated in Figure 4.13b, it can be concluded that the distance ratio for a reasonable cut should be relatively high among the candidate cut set under the limitation of step 3. In addition, when each possible candidate cut connects to the shape contour, it should form a closed curve. The area of this closed curve can be calculated and used to identify the whole leg or antennae to be pruned. Using this idea, the shape decomposition algorithm is presented below.

In the left segment and right segment respectively, we use the candidate cut sets which are found by applying (4.25) and (4.26) separately to the candidate cut set. The candidate cut set is

47

truncated further by using the distance ratio limited by parameter γ (Eqn. 4.27 and 4.28). After truncation, the reduced cut set is sorted in descending order.

$$C_{\gamma,\delta,a}(L) = \{cut_1 \ldots cut_p\}, \qquad r_1 \geq \cdots \geq r_p \geq \gamma, R_1, \ldots, R_p < \delta, a_{cut_1} = \cdots = a_{cut_p} = 0 \quad (4.27)$$

$$C_{\gamma,\delta,a}(R) = \{cut_1 \ldots cut_q\}, \qquad r_1 \geq \cdots \geq r_q \geq \gamma, R_1, \ldots, R_q < \delta, a_{cut_1} = \cdots = a_{cut_q} = 0 \quad (4.28)$$

As mentioned above, the distance ratio for a reasonable cut should be relatively high. So we introduce another parameter, selection ratio μ, to truncate the candidate cut set to the top $1/\mu$ cuts.

$$C_{\delta,a,\gamma,\mu}(L) = \left\{ cut_1 \ldots cut_{\left\lceil \frac{p}{\mu} \right\rceil} \right\},$$

$$R_1, \ldots, R_{\left\lceil \frac{p}{\mu} \right\rceil} < \delta, a_{cut_1} = \cdots = a_{cut_{\left\lceil \frac{p}{\mu} \right\rceil}} = 0, r_1 \geq \cdots \geq r_{\left\lceil \frac{p}{\mu} \right\rceil} \geq \gamma \qquad (4.29)$$

$$C_{\delta,a,\gamma,\mu}(R) = \left\{ cut_1 \ldots cut_{\left\lceil \frac{q}{\mu} \right\rceil} \right\},$$

$$R_1, \ldots, R_{\left\lceil \frac{q}{\mu} \right\rceil} < \delta, a_{cut_1} = \cdots = a_{cut_{\left\lceil \frac{q}{\mu} \right\rceil}} = 0, r_1 \geq \cdots \geq r_{\left\lceil \frac{q}{\mu} \right\rceil} \geq \gamma \qquad (4.30)$$

For the candidate cut set determined by equations 4.29 and 4.30, the closed curve area is calculated for each possible cut line. The two points whose connection creates the biggest area are used to make the first cut on the left side and on the right side (Figure 4.14).

(a)   (b)
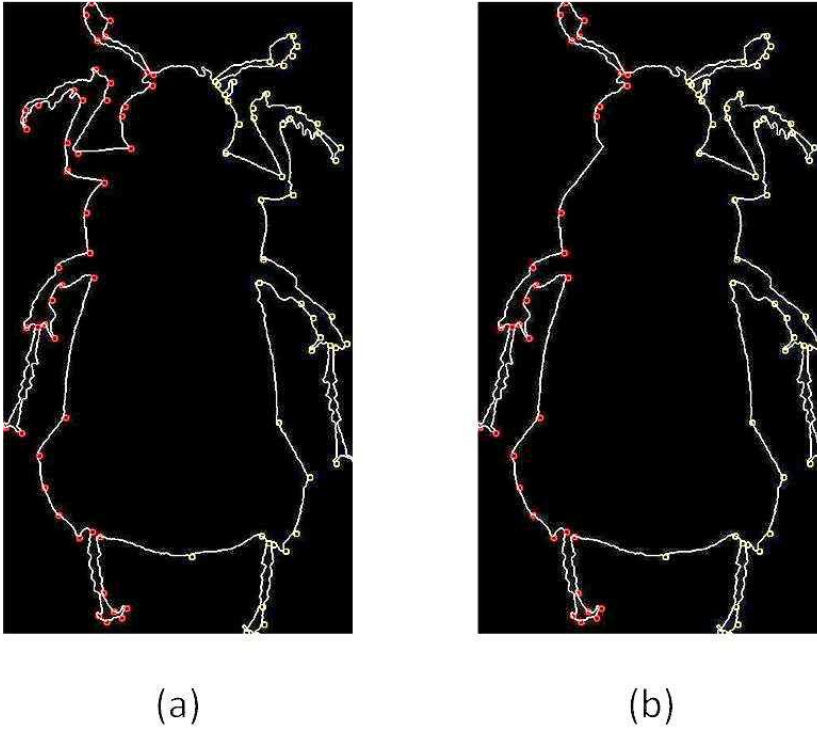
Figure 4.14: Representative image showing candidate connection point set result from (a) visual curvature result on boundary shape; (b) shape after first cut on the left side.

- Step 5: After the first cut is made, the set of candidate connection points has been changed due to the removal of an area segment. Two candidate points where the cut was made have been removed as well as the candidate points on the contour between these two points. Because the candidate point set has been updated, the algorithm can be repeated starting with step 3 to construct new possible candidate cuts. The algorithm on the left side will end when the number of cuts reaches 4 or there is no possible cut to satisfy all limitations set by thresholds γ, δ, α and μ. The algorithm will then proceed to the right side and prune up to 4 more areas.

The insect shape decomposition example shown in Figure 4.15 uses ABB #2 image. The thresholds used in the algorithm are $\gamma = 2.5, \delta = 1/10, \alpha = 0$ and $\mu = 2$. Additional results of

shape decomposition using this procedure are shown in Figure 4.16 through Figure 4.20 using the same threshold values.
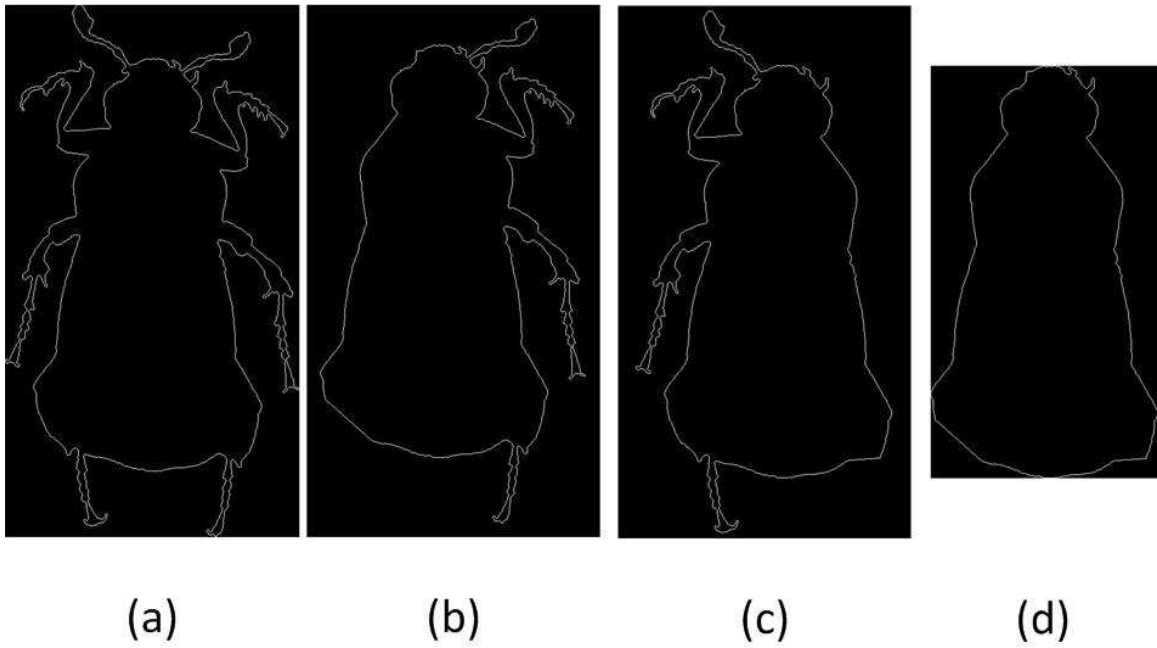
Figure 4.15: Results of image pruning for #2 image (a) Original boundary shape; (b) left side shape decomposition; (c) right side shape decomposition (d) final insect shape decomposition result.

(a)
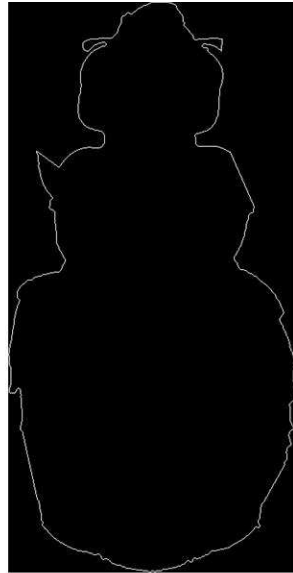
(b)

Figure 4.16: Results of image pruning for #4 image (a) Original boundary shape; (b) insect shape decomposition result.
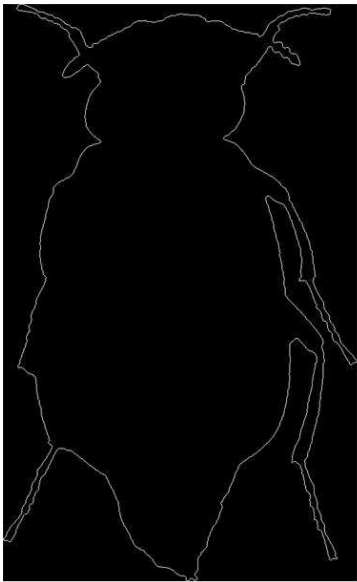
(a)
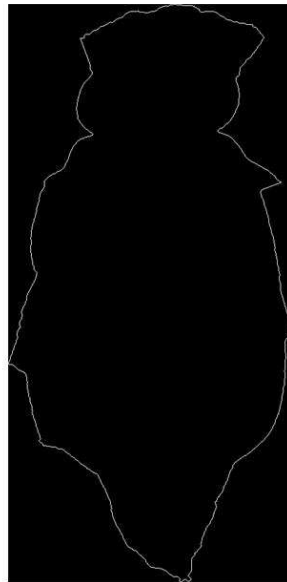
(b)

Figure 4.17: Results of image pruning for #24 image (a) Original boundary shape; (b) insect shape decomposition result.

(a)   (b)
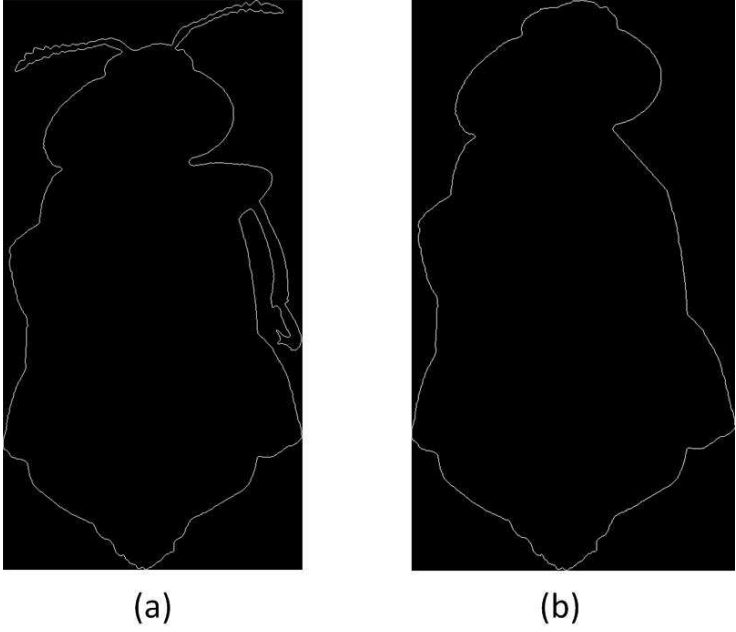
Figure 4.18: Results of image pruning for #26 image (a) Original boundary shape; (b) insect

shape decomposition result.

(a)   (b)
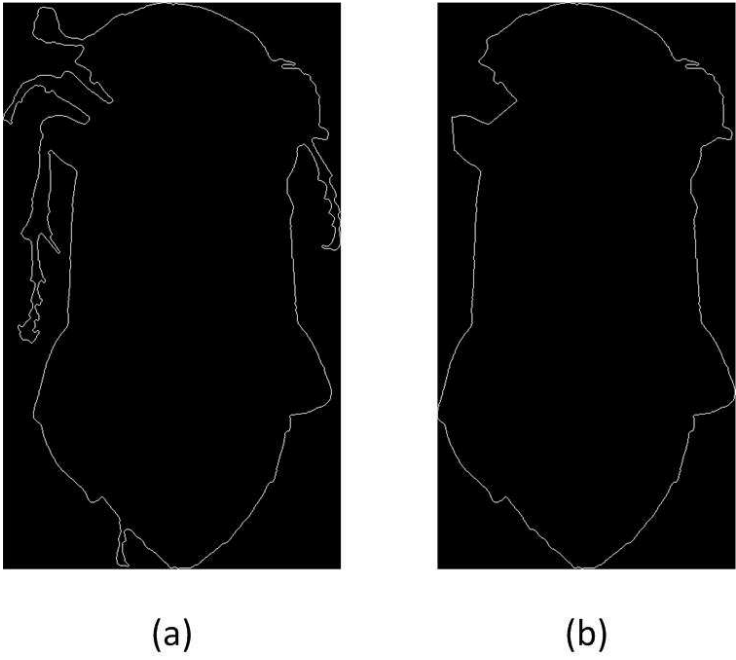
Figure 4.19: Results of image pruning for #36 image (a) Original boundary shape; (b) insect

shape decomposition result.

(a)   (b)
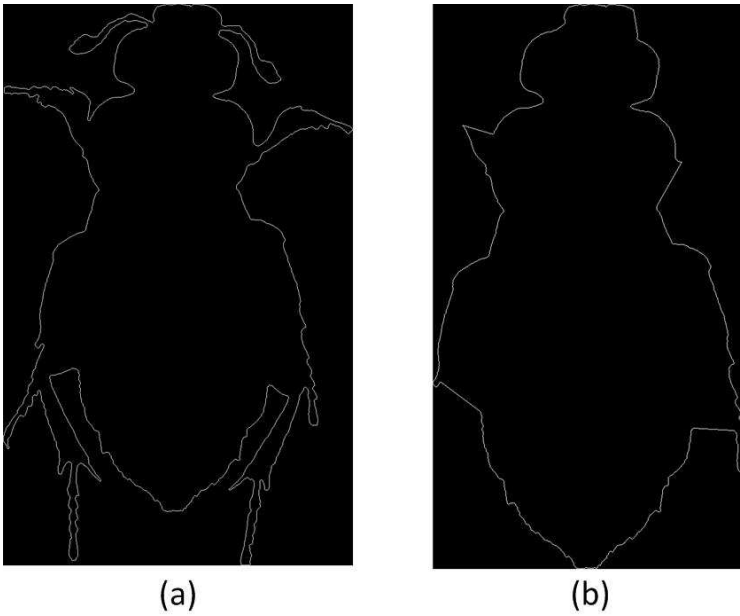
Figure 4.20: Results of image pruning for #41 image (a) Original boundary shape; (b) insect shape decomposition result.

4.4 Experimental Analysis

When using images where the legs and antennae are manually pruned insect overall classification accuracy for 11 species of insects reached 78% using the Fourier descriptor method and 72% using the area component method. After applying the visual curvature and shape decomposition algorithm to remove uncertainty introduced by legs and antennae, the overall classification accuracies increased to 67% using the Fourier descriptor method and 76% using the area component method when using the best combination of threshold parameters (Table 4.3).

Visual curvature parameters		Shape Decomposition parameters			Classification Accuracy			
					Fourier descriptor		Area component	
ε	K	γ	δ	μ	ABB	Overall	ABB	Overall
0.015	10	4	1/10	1	0.80	0.62	0.60	0.72
0.010	10	4	1/10	1	0.80	0.55	0.60	0.72
0.015	10	3	1/10	1	0.80	0.64	0.60	0.74
0.010	10	3	1/10	1	0.80	0.59	0.60	0.71
0.015	10	2.5	1/10	2	0.90	0.67	0.60	0.76
0.010	10	2.5	1/10	2	0.80	0.57	0.60	0.73
0.015	10	2.5	1/10	1.5	0.90	0.63	0.60	0.75
0.010	10	2.5	1/10	1.5	0.50	0.57	0.40	0.70
0.015	10	2	1/10	2	0.90	0.68	0.60	0.74
0.010	10	2	1/10	2	0.60	0.62	0.60	0.73
0.015	10	2	1/10	1.5	0.90	0.63	0.60	0.73
0.010	10	2	1/10	1.5	0.70	0.54	0.60	0.73

Table 4.3: Effect of visual curvature and shape decomposition parameters on classification accuracy on automatically decomposed shapes using Fourier descriptors and Area components methods for 11 species of insects (N=92).

Thresholds set by $\varepsilon = 0.015, K = 10$ in visual curvature computation and thresholds set by $\gamma = 2.5, \delta = 1/10, \alpha = 0, \mu = 2$ in shape decomposition algorithm yielded the most robust classification results. Classification accuracy of ABB was 90% when using Fourier descriptors on the images subject to automatic decomposition compared to 80% on the manually decomposed images. Classification accuracy of ABB using automatic decomposition and area components was 60% which was the same as realized from manual decomposition (Table 4.4).

	Fourier Descriptor		Area Component	
Classification image source	ABB	Overall	ABB	Overall
Original shape	30%	57%	60%	64%
Manual decomposition	80%	78%	60%	72%
Automatic decomposition	90%	67%	60%	76%

Table 4.4: Insect classification accuracy comparison between original shapes and manually and automatically decomposed images using Fourier descriptor and area component methods for ABB and 11 species (N=92).

This insect shape decomposition algorithm based on visual curvature computation is shown to be useful. The classification accuracies have been dramatically improved compared with those of the original shapes. The data show that the classification accuracy of the automatically pruned shapes approaches that of manually pruned shapes. ABB classification accuracy was 90% using the Fourier descriptor method.

4.5 Parameter Selection

Based on the results of several trials using different parameters, this algorithm was shown to be sensitive to parameter selection. The visual curvature algorithm selects the set of candidate attachment points which have the largest visual curvature. A good visual curvature result should include all real attachment points with minimum false positives. In the shape decomposition algorithm, due to the uncertainty of the candidate set, three parameters were used to fine-tune the set of candidate points. Because a cut is made by linking two candidate attachment points, the most important thing for a correct cut is that the two candidate attachment points be within the same leg or antenna portion of the entire shape.

This intuitive insect shape decomposition algorithm removes insect legs and antennas automatically when using appropriate parameters. The classification accuracy achieves the level of manual decomposed shapes which means that the decomposed shape is sufficient for classification work. However, both the Fourier descriptor and area component methods do not reach high accuracies, only 67% and 76%, respectively. Instead of using two methods separately, one possible solution is to combine them together so they can complement each other for insect classification. Thus, a hybrid region-based and contour-based approach is proposed in Chapter 5.

CHAPTER V

HYBIRD REGION-BASED AND CONTOUR-BASED APPROACH

In previous chapters, region-based and contour-based methods applied separately achieved classification accuracies 64% and 57% respectively. To avoid uncertainty introduced by the insect's legs and antennae, a shape decomposition algorithm was proposed to remove those shape distractors automatically. This encouragingly improved classification accuracy to 76 and 67% on region-based and contour-based methods respectively on the cleaned shapes. However, both area components and Fourier descriptor methods could not yield satisfactory classification results when using each of them independently. After more observations of misclassification cases, it was found that the two methods could be complementary to each other, meaning that combining them together could be a good approach to further increase the classification accuracy. With this idea, a hybrid region-based and contour-based approach is developed in this chapter.

Many mathematical theories have been applied for decision fusion-based classification. Fuzzy set theory [9], Dempster-Shafer theory [52], Bayes fusion [53], belief approach [54], joint likelihood and the weighted majority [55], possibility and evidence theory [56] and multiple kernel learning method [57] have thoroughly studied the results of combining different classifiers. In this chapter, fuzzy set theory is used to combine two features of the decomposed shape and the fusion rule proposed by Fauvel [9] is implemented for the classification of insect images. Detailed classification results from this approach are presented and discussed.

5.1 Fuzzy Set Theory for Decision Fusion

In traditional binary set theory, a membership value of 1 is assigned to elements which are in the set, and 0 is assigned to elements which are outside the set. Fuzzy set theory, first introduced by Zadeh [58], defines the concept of partial membership, and thus the membership degree can range from 0 to 1. With the ability to handle ambiguity within data, fuzzy set theory is widely used for additional processing of outputs from multiple classifiers [9]. Specifically, we implement the decision fusion algorithm based on fuzzy set theory in this investigation.

5.1.1 Definitions [9]

A fuzzy set F of a reference set U is a set of ordered pairs:

$$F = \{(x, \mu_F(x)) | x \in U\} \tag{5.1}$$

And $\mu_F: U \rightarrow [0,1]$ is the membership function of F in U.

A fuzzy set is a normal set if and only if:

$$\max \mu_F(x) = 1 \tag{5.2}$$

The support of a fuzzy set F is:

$$Supp(F) = \{x \in U | \mu_F(x) > 0\} \tag{5.3}$$

5.1.2 Measure of Fuzziness [59]

Pal et al. [59] proposed a measure of fuzziness on multiplicative class.

$$H(\mu_F) = K \sum_{i=1}^{n} g(\mu_F(x_i)), K \epsilon R^+ \tag{5.4}$$

Where $g(\mu_F)$ is defined as:

$$\begin{cases} g(t) = \tilde{g}(t) - \min_{0 \leq t \leq 1} \tilde{g}(t) \\ \tilde{g}(t) = h(t)h(1-t) \end{cases} \tag{5.5}$$

And h is the concave increasing function.

$$h: [0,1] \rightarrow R^2, \forall x \in [0,1] \ h'(x) > 0 \text{ and } h''(x) < 0 \tag{5.6}$$

Different choices of function g will lead to various measure definitions. In this investigation, let $h: [0,1] \rightarrow R^+$ be $h(t) = t^\alpha, 0 < \alpha < 1$. And the function, $called \ \alpha - Q$uadratic entropy, is a measure of fuzziness.

$$H_{\alpha QE}(\mu_F) = \frac{1}{n2^{-2\alpha}} \sum_{i=1}^{n} \mu_F(x_i)^\alpha (1 - \mu_F(x_i))^\alpha \tag{5.7}$$

5.2 Decision Fusion for Insect Classification

In this investigation, after feature extraction of all insect images using region-based and contour-based methods, for an individual image P, the Euclidean distance between its feature vector and the mean feature vector of all n species is calculated according to equation 5.8:

$$d(P) = \{d^j(P), j = 1, 2, \dots, n\} \tag{5.8}$$

To be considered a fuzzy set, the value of each element must range from 0 to 1, so normalization of the distance vector is required using equation 5.9:

$$D^j(P) = 1 - \frac{d^j(P) - p}{p - q}, \text{ where } p = \max[d(P)] \text{ and } q = \min[d(P)] \tag{5.9}$$

$$D(P) = \{D^j(P), j = 1, 2, \dots, n\} \tag{5.10}$$

For a given image P, the output of classifier i is defined as the fuzzy set given by:

$$\pi_i(P) = \{D_i^j(P), j = 1, 2, \dots, n\} \tag{5.11}$$

Where $D_i^j(P) \in [0,1]$ is the membership degree of image P to class j using classifier i. By definition, the larger the D_i^j value is, the more likely it is that this image belongs to class j. With

58

different classifiers, m fuzzy sets are computed for each image which are then input to the fusion process.

$$\pi = \{\pi_1(P), \pi_2(P), \dots, \pi_m(P)\} \tag{5.12}$$

As discussed in Chapters 3 and 4, 11 different insect species comprising a total of 92 images correspond to 11 classes, and two different contour representation methods correspond to 2 fuzzy sets.

The hybrid region-based and contour-based approaches for classification of each image are organized as follows [9]:

- Step 1: For each image P, $\pi = \{\pi_1(P), \pi_2(P)\}$ fuzzy sets are constructed according to equations 5.8 to 5.12.

- Step 2: For each fuzzy set, the fuzziness degree H is computed. Specifically, based on the rewriting of equation 5.7, the $\alpha -$ Quadratic entropy [59] calculated by equations 5.13 and 5.14 is implemented which provides a measure of the fuzziness in each classifier.

$$S_i^j(P) = \frac{D_i^j(P)^\alpha \left(1 - D_i^j(P)\right)^\alpha}{2^{-2\alpha}}, i \in [1,2], j \in [1,11] \tag{5.13}$$

$$H_i(P) = \frac{1}{n} \sum_{j=1}^{n} S_i^j(P), \qquad i \in [1,2], j \in [1,11] \tag{5.14}$$

The parameter α differentiates the degree of fuzziness for different membership degree values. When the parameter is close to 0, fuzzy measure is not sensitive to changes in $D_i^j(P)$ and all the fuzzy sets have approximately the same degree of fuzziness [9].

- Step 3: Intuitively, the classifier is most reliable when one class has a relatively high membership value and all other classes have membership values closer to 0. It follows that if all of the classes have membership values that are approximately the same it

indicates significant ambiguity and the classifier is considered unreliable. In other words, uncertain results are obtained using the classifier which produces a high degree of fuzziness. To reduce classifier uncertainty, each fuzzy set is weighted by:

$$w_i(P) = \frac{\sum_{k=1,k\neq i}^{m} H_i(P)}{(m-1)\sum_{i=1}^{m} H_i(P)}, \sum_{i=1}^{m} w_i = 1 \qquad (5.15)$$

- Step 4: Next, the combination operator is applied to image P to make the fusion decision. After applying each classifier's fuzzy set weight to its corresponding distance vector, given by equation 5.15, a new distance vector is constructed combining region-based and contour-based methods:

$$\mu(P) = \max\{w_1 d_1^1(P), w_1 d_1^2(P), \dots, w_1 d_1^{11}(P), w_2 d_2^1(P), w_2 d_2^2(P), \dots, w_2 d_2^{11}(P)\} \quad (5.16)$$

Where $d_i^j(P)$ is the Euclidean distance between image P's feature vector to the j class representative feature vector using classifier i. $\mu(P)$ represents the largest membership degree after the combination rule is applied for two classifiers and 11 classes.

- Step 5: Finally, the class is selected corresponding to the highest membership value.

5.3 Experimental Results and Analysis

As described in step 2 above, to evaluate reliability, the $q$uadratic entropy is calculated first to measure fuzziness of the two classifiers. After that, as shown in step 3, the weight of each classifier is calculated by equation 5.15 to reduce classifier uncertainty. The significance of the weighting is to emphasize the classifier having less fuzziness and somehow neglect the classifier with more fuzziness. In other words, a high weight is given to the reliable classifier and a low weight to the unreliable classifier so that the final combined classifier takes advantage of them both. The sum of the weights of two classifiers is equal to 1.

For example, for a certain image which belongs to class 2, the class representation using two classifiers is presented as figure 5.1.
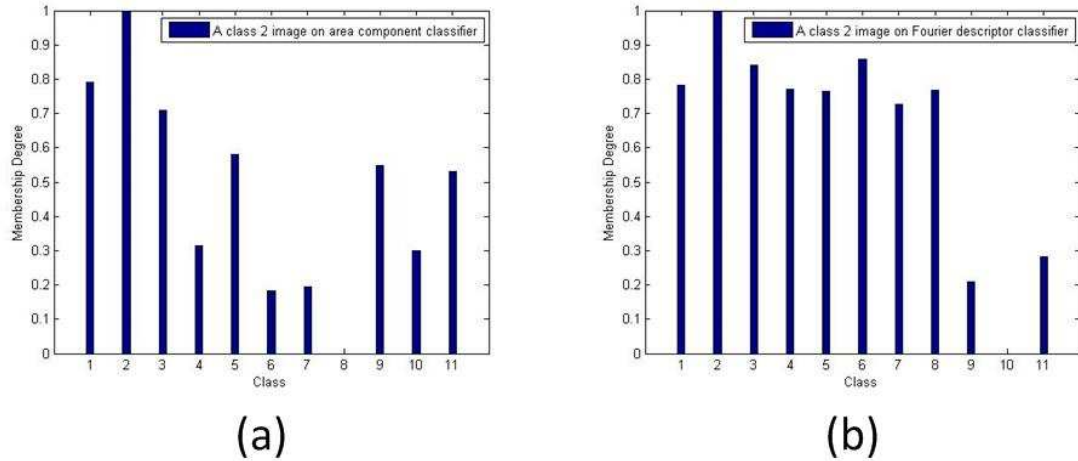
Figure 5.1: Class membership degrees for an example image in class 2 (a) using area component classifier; (b) using Fourier descriptor classifier.

Both classifiers could classify this image into class 2 with their highest membership degree. However, intuitively, we could conclude that the fuzziness of the area component classifier is less than that of the Fourier descriptor classifier. In other words, for this image classification, classifier 1 is more reliable than classifier 2. Classifier 2 has more uncertainty even though it could make the right classification. Under this condition, more weight is placed on results of classifier 1 and less weight on classifier 2.

In this $\alpha -$ Quadratic entropy fuzziness measurement, for each image, through equations 5.13 to 5.15, the weight is affected by its membership degrees in two classifiers and the parameter α $(0 < \alpha < 1)$ value as well. Specifically, for the example image in class 2, the weight distribution for two classifiers is shown in figure 5.2 as the α parameter is changing.
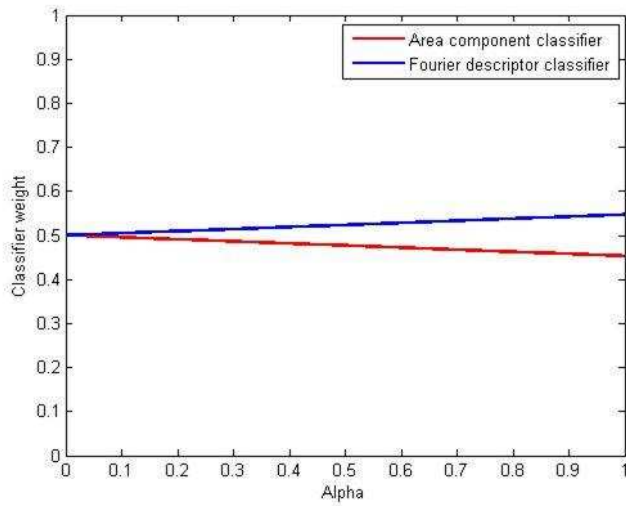
Figure 5.2: The weights for two classifiers for an image in class 2 for different values of α.

As discussed above, for this image, it is preferred to emphasize the area component classifier as well as reduce the influence of the Fourier descriptor classification. From figure 5.2, the goal is achieved when the parameter α approaches 0. When applied to all images in the training data set, the optimal value of α, which differentiates the degree of fuzziness for different membership degree values, is approximately equal to 0 and this produces the best classification accuracy (Table 5.1).

Parameter α	10^(-17)	0.1	0.2	0.3	0.4	0.5	0.6	0.7	0.8	0.9	0.99
ABB Accuracy	100%	60%	60%	60%	60%	60%	60%	60%	60%	60%	60%
Overall Accuracy	90%	64%	64%	61%	62%	60%	60%	60%	60%	60%	60%

Table 5.1: Classification accuracies for ABB and 11 species (N=92) using different α parameter values.

Based on the selection of parameter α, the classification accuracy for ABB was 100% and overall classification accuracy for all 11 species was 90% (Table 5.2).

Methods	S1	S2	S3	S4	S5	S6	S7	S8	S9	S10	S11	Overall
Hybrid	100%	89%	70%	70%	100%	83%	90%	83%	100%	100%	100%	90%
Area Comp.	60%	89%	70%	60%	83%	83%	50%	67%	100%	88%	88%	76%
Fourier Des.	90%	78%	30%	20%	50%	50%	60%	67%	100%	100%	88%	67%

Table 5.2: Classification accuracies for hybrid region-based and contour-based approach on images with legs and antennae automatically removed. S1 represents the American Burying Beetle (ABB).

The hybrid fusion method compared to area components and Fourier descriptor methods separately resulted in improved overall classification accuracy for the current data set. In all cases the hybrid decision fusion operator was successful in keeping the best classification results determined separately by the two methods. In addition, for S1, S4, S5, S7, S8 and S11, the hybrid classification accuracy is higher than either of the methods individually. The hypothesis that each method could be complementary to the other method was confirmed by using this hybrid region-based and contour-based approach.

5.4 Experimental Results and Analysis of Leave-one-out Validation

To further test the robustness of our algorithm, we implemented the leave-one-out validation. In other words, each test image is not involved in the training stage when the average feature vector is computed from multiple samples of each class. The experimental results are shown in Table 5.3, where both ABB and overall classification accuracies decrease significantly compared with Table 5.2. Still it is shown that cleaned shapes after decomposition are preferred for better classification. Further, the decision fusion is able to improve the classification accuracy for ABB (80%) and all species (61%), as shown in Table 5.4.

	Area Component		Fourier Descriptor	
Classification image source	ABB	Overall	ABB	Overall
Original shape	40%	35%	10%	33%
Manual decomposition	50%	41%	80%	63%
Automatic decomposition	50%	35%	80%	43%

Table 5.3: Classification results of leave-one-out validation for ABB and 11 species (N=92).

Methods	S1	S2	S3	S4	S5	S6	S7	S8	S9	S10	S11	Overall
Hybrid	80%	89%	30%	30%	17%	67%	50%	50%	89%	100%	75%	61%
Area Comp.	50%	44%	30%	20%	0%	50%	10%	33%	89%	38%	26%	35%
Fourier Des.	80%	78%	10%	10%	17%	33%	50%	17%	0%	100%	75%	43%

Table 5.4: Fusion results of leave-one-out validation. S1 represents the American Burying Beetle

(ABB).

With the decreasing of classification accuracies in both methods, we could conclude that the

robust classification result may not be achieved only with these two shape representation methods

in practice. However, our proposed insect shape decomposition algorithm could still improve

classification accuracies in both methods for ABB and overall species. There are three thoughts

for future research from this leave-one-out validation experiment. First, we may need additional

features (such as colors, edges or textures) to improve the accuracy and robustness of the

algorithm. Second, we also need more training samples for each species to improve the

representativeness of shape features. Third, we may need involve advanced feature learning [60]

to learn more stable features for each species.

CHAPTER VI

CONCLUSIONS AND FUTURE WORK

In this investigation, an insect classification algorithm was implemented through template matching. Specifically, shape features were extracted from color images for analysis and classification based on binary images. After image preprocessing and insect object extraction and alignment, a region-based area component method and a contour-based Fourier descriptor method were implemented to classify 11 different of types of insects to species from a total of 92 images. Due to the shape uncertainty introduced by the position of the legs and antennae of the insects, initial classification accuracy was not sufficient for the intended purpose. Using visual curvature theory, an intuitive insect shape decomposition algorithm was proposed to cut the legs and antennae from insect body shapes automatically. Experimental results using the same region-based and contour-based methods on the decomposed shapes demonstrated that the algorithm was useful in removing uncertainty in the insect shape by increasing classification accuracy by 12% and 10% respectively. Moreover, classification accuracy was dramatically improved to 90% using the Fourier descriptor approach on American Burying Beetle (ABB) specimens. To achieve higher overall classification accuracy, a hybrid approach using a fusion operator to combine region-based and contour-based methods together was proposed. After that implementation, the overall accuracy achieved 90% and the ABB classification accuracy increased to 100%. However, the experimental results of leave-one-out validation show that the proposed algorithm still needs future improvements in three areas. First, additional features (such as colors, edges or textures) are needed to complement shape-based ones. Second, more training samples and a large

65

data set are necessary to improve the overall performance of the proposed algorithm. Third, advanced feature learning may be helpful to find reliable features for each species.

The original objective of the algorithm was to classify and identify the American Burying Beetle (ABB) precisely and also be able to discriminate other species of interest as well. There are still rooms to improve the overall insect classification accuracy and robustness. Furthermore, the methods developed in this investigation may have application for other insect assemblages, and even on non-insect animals, where unsupervised classification is desired.

REFERENCES

1.   Liu, H., et al. *Visual curvature*. in *Computer Vision and Pattern Recognition, 2007. CVPR'07. IEEE Conference on*. 2007. IEEE.

2.   Ratcliffe, B.C., *carrion beetles (Coleoptera: Silphidae) of Nebraska.* 1996.

3.   Mountain-Prairie, U. *File: American Burying Beetle.jpg https://www.flickr.com/photos/51986662@N05/7489195168*.

4.   Hardin, J., *American Burying Beetle trap monitor proposal*.

5.   Liu, H., W. Liu, and L.J. Latecki. *Convex shape decomposition*. in *Computer Vision and Pattern Recognition (CVPR), 2010 IEEE Conference on*. 2010. IEEE.

6.   Latecki, L.J. and R. Lakämper, *Convexity rule for shape decomposition based on discrete contour evolution.* Computer Vision and Image Understanding, 1999. **73**(3): p. 441-454.

7.   Ren, Z., J. Yuan, and W. Liu, *Minimum near-convex shape decomposition.* 2013.

8.   Ghosh, M., et al., *Fast approximate convex decomposition using relative concavity.* Computer-Aided Design, 2013. **45**(2): p. 494-504.

9.   Fauvel, M., J. Chanussot, and J.A. Benediktsson, *Decision fusion for the classification of urban remote sensing images.* Geoscience and Remote Sensing, IEEE Transactions on, 2006. **44**(10): p. 2828-2838.

10.   Larios, N., et al., *Automated insect identification through concatenated histograms of local appearance features: feature vector generation and region detection for deformable objects.* Machine Vision and Applications, 2008. **19**(2): p. 105-123.

11. Kuhl, F.P. and C.R. Giardina, *Elliptic Fourier features of a closed contour.* Computer graphics and image processing, 1982. **18**(3): p. 236-258.

12. Cho, J., et al., *Automatic identification of whiteflies, aphids and thrips in greenhouse based on image analysis.* Red, 2007. **346**(246): p. 244.

13. Mayo, M. and A.T. Watson, *Automatic species identification of live moths.* Knowledge-Based Systems, 2007. **20**(2): p. 195-202.

14. Zayas, I. and P. Flinn, *Detection of insects in bulk wheat samples with machine vision.* Transactions of the ASAE-American Society of Agricultural Engineers, 1998. **41**(3): p. 883-888.

15. Al-Saqer, S., et al., *Identification of pecan weevils through image processing.* American Journal of Agricultural and Biological Sciences, 2010. **6**(1): p. 69.

16. Arbuckle, T., et al. *Biodiversity informatics in action: identification and monitoring of bee species using ABIS.* in *Proc. 15th Int. Symp. Informatics for Environmental Protection.* 2001. Citeseer.

17. Watson, A.T., M.A. O'Neill, and I.J. Kitching, *Automated identification of live moths (Macrolepidoptera) using digital automated identification system (daisy).* Systematics and Biodiversity, 2004. **1**(3): p. 287-300.

18. Lowe, D.G., *Distinctive image features from scale-invariant keypoints.* International journal of computer vision, 2004. **60**(2): p. 91-110.

19. Zhang, D. and G. Lu, *Review of shape representation and description techniques.* Pattern recognition, 2004. **37**(1): p. 1-19.

20. Hu, M.-K., *Visual pattern recognition by moment invariants.* Information Theory, IRE Transactions on, 1962. **8**(2): p. 179-187.

21. Ezer, N., E. Anarim, and B. Sankur. *A comparative study of moment invariants and fourier descriptors in planar shape recognition.* in *Electrotechnical Conference, 1994. Proceedings., 7th Mediterranean.* 1994. IEEE.

22. Park, J.-S. and T. Kim, *Shape-based image retrieval using invariant features*, in *Advances in Multimedia Information Processing-PCM 2004.* 2005, Springer. p. 146-153.

23. Gonzalez, R.C., R.E. Woods, and S.L. Eddins, *Digital image processing using MATLAB.* 2004: Pearson Education India.

24.   Khotanzad, A. and Y.H. Hong, *Invariant image recognition by Zernike moments.* Pattern Analysis and Machine Intelligence, IEEE Transactions on, 1990. **12**(5): p. 489-497.

25.   Li, S., M.-C. Lee, and C.-M. Pun, *Complex Zernike moments features for shape-based image retrieval.* Systems, Man and Cybernetics, Part A: Systems and Humans, IEEE Transactions on, 2009. **39**(1): p. 227-237.

26.   Bunke, H. and U. Bühler, *Applications of approximate string matching to 2D shape recognition.* Pattern recognition, 1993. **26**(12): p. 1797-1812.

27.   Kim, H.-K. and J.-D. Kim, *Region-based shape descriptor invariant to rotation, scale and translation.* Signal Processing: Image Communication, 2000. **16**(1): p. 87-93.

28.   Zhang, D. and M.C.Y. Lim. *An efficient and robust technique for region based shape representation and retrieval.* in *Computer and Information Science, 2007. ICIS 2007. 6th IEEE/ACIS International Conference on*. 2007. IEEE.

29.   Arbter, K., *Affine-invariant Fourier descriptors.* From Pixels to Features, 1989: p. 153-164.

30.   Granlund, G.H., *Fourier preprocessing for hand print character recognition.* Computers, IEEE Transactions on, 1972. **100**(2): p. 195-201.

31.   El-ghazal, A., O. Basir, and S. Belkasim, *Farthest point distance: A new shape signature for Fourier descriptors.* Signal Processing: Image Communication, 2009. **24**(7): p. 572-586.

32.   Kunttu, I. and L. Lepisto, *Shape-based retrieval of industrial surface defects using angular radius Fourier descriptor.* Image Processing, IET, 2007. **1**(2): p. 231-236.

33.   Yang, H.S., S.U. Lee, and K.M. Lee, *Recognition of 2D object contours using starting-point-independent wavelet coefficient matching.* Journal of Visual Communication and Image Representation, 1998. **9**(2): p. 171-181.

34.   Belongie, S., J. Malik, and J. Puzicha. *Shape context: A new descriptor for shape matching and object recognition.* in *NIPS*. 2000.

35.   Belongie, S., J. Malik, and J. Puzicha, *Shape matching and object recognition using shape contexts.* Pattern Analysis and Machine Intelligence, IEEE Transactions on, 2002. **24**(4): p. 509-522.

36.   Freeman, H., *On the encoding of arbitrary geometric configurations.* Electronic Computers, IRE Transactions on, 1961(2): p. 260-268.

37.   Lee, D.-J., S. Antani, and L.R. Long. *Similarity measurement using polygon curve representation and fourier descriptors for shape-based vertebral image retrieval*. in *Medical Imaging 2003*. 2003. International Society for Optics and Photonics.

38.   Arica, N. and F.Y. Vural. *A shape descriptor based on circular Hidden Markov Model*. in *Pattern Recognition, 2000. Proceedings. 15th International Conference on*. 2000. IEEE.

39.   Kim, D.H., I.D. Yun, and S.U. Lee, *A new shape decomposition scheme for graph-based representation.* Pattern Recognition, 2005. **38**(5): p. 673-689.

40.   Mi, X. and D. DeCarlo. *Separating parts from 2d shapes using relatability*. in *Computer Vision, 2007. ICCV 2007. IEEE 11th International Conference on*. 2007. IEEE.

41.   Lu, G. and A. Sajjanhar, *Region-based shape representation and similarity measure suitable for content-based image retrieval.* Multimedia Systems, 1999. **7**(2): p. 165-174.

42.   Tieng, Q.M. and W. Boles, *Recognition of 2D object contours using the wavelet transform zero-crossing representation.* IEEE Transactions on Pattern Analysis and Machine Intelligence, 1997. **19**(8): p. 910-916.

43.   Zhang, D. and G. Lu. *A comparative study of Fourier descriptors for shape representation and retrieval*. in *Proceedings of the Fifth Asian Conf. on Computer Vision*. 2002. Citeseer.

44.   Sarfraz, M. *Object recognition using fourier descriptors: Some experiments and observations*. in *Computer Graphics, Imaging and Visualisation, 2006 International Conference on*. 2006. IEEE.

45.   Zhang, D. and G. Lu, *Study and evaluation of different Fourier methods for image retrieval.* Image and Vision Computing, 2005. **23**(1): p. 33-49.

46.   Zhang, D. and G. Lu. *Content-Based Shape Retrieval Using Different Shape Descriptors: A Comparative Study*. in *ICME*. 2001.

47.   He, X.C. and N.H. Yung, *Corner detector based on global and local curvature properties.* Optical Engineering, 2008. **47**(5): p. 057008-057008-12.

48.   Sonthi, R., G. Kunjur, and R. Gadh. *Shape feature determination usiang the curvature region representation*. in *Proceedings of the fourth ACM symposium on Solid modeling and applications*. 1997. ACM.

49.   Mokhtarian, F. and A.K. Mackworth, *A theory of multiscale, curvature-based shape representation for planar curves.* IEEE Transactions on Pattern Analysis and Machine Intelligence, 1992. **14**(8): p. 789-805.

50.   Dudek, G. and J.K. Tsotsos, *Shape representation and recognition from multiscale curvature.* Computer Vision and Image Understanding, 1997. **68**(2): p. 170-189.

51.   He, X.-C. and N.H. Yung. *Curvature scale space corner detector with adaptive threshold and dynamic region of support.* in *Pattern Recognition, 2004. ICPR 2004. Proceedings of the 17th International Conference on.* 2004. IEEE.

52.   Fontani, M., et al., *A framework for decision fusion in image forensics based on Dempster-Shafer theory of evidence.* 2013.

53.   Shi, X. and R. Manduchi. *A study on Bayes feature fusion for image classification.* in *Computer Vision and Pattern Recognition Workshop, 2003. CVPRW'03. Conference on.* 2003. IEEE.

54.   Laanaya, H., et al. *Classifier fusion for post-classification of textured images.* in *Information Fusion, 2008 11th International Conference on.* 2008. IEEE.

55.   Jeon, B. and D.A. Landgrebe, *Decision fusion approach for multitemporal classification.* Geoscience and Remote Sensing, IEEE Transactions on, 1999. **37**(3): p. 1227-1233.

56.   Martin, A. *Comparative study of information fusion methods for sonar images classification.* in *Information Fusion, 2005 8th International Conference on.* 2005. IEEE.

57.   Gehler, P. and S. Nowozin. *On feature combination for multiclass object classification.* in *Computer Vision, 2009 IEEE 12th International Conference on.* 2009. IEEE.

58.   Zadeh, L.A., *Fuzzy sets.* Information and control, 1965. **8**(3): p. 338-353.

59.   Pal, N.R. and J.C. Bezdek, *Measuring fuzzy uncertainty.* Fuzzy Systems, IEEE Transactions on, 1994. **2**(2): p. 107-118.

60.   Bengio, Y., A. Courville, and P. Vincent, *Representation learning: A review and new perspectives.* Pattern Analysis and Machine Intelligence, IEEE Transactions on, 2013. **35**(8): p. 1798-1828.

VITA

Bo Li

Candidate for the Degree of

Master of Science

Thesis: SHAPE-BASED INSECT CLASSIFICATION: A HYBRID REGION-BASED
AND CONTOUR-BASED APPROACH

Major Field: Electrical Engineering

Biographical:

Education:

Completed the requirements for the Bachelor of Science in Electronic
Information Science and Technology at Shandong University, Jinan, Shandong,
China in 2009.

Experience:

Visual Computing and Image Processing Lab (VCIPL), OSU Stillwater, OK
Research Assistant,   Jan.2013—Present.

Professional Memberships:

IEEE Student Member